JCI insight

Essential role of obscurin kinase-1 in cardiomyocyte coupling via N-cadherin phosphorylation

Li Wang, … , Nathan T. Wright, Aikaterini Kontrogianni-Konstantopoulos

JCI Insight. 2023. https://doi.org/10.1172/jci.insight.162178.

Research In-Press Preview **Cell biology**

Obscurins are giant cytoskeletal proteins with structural and regulatory roles. Obscurin-B (~870 kDa), the largest known isoform, contains two enzymatically active Ser/Thr kinase (kin) domains, kin1 and kin2, which belong to the myosin light chain kinase (MLCK) family. Kin1 binds to and phosphorylates N-cadherin, a major component of the intercalated disc (ICD), the unique sarcolemmal microdomain that mediates the mechanochemical coupling of adjacent cardiomyocytes. Obscurin-B containing kin1 and N-cadherin co-localize at cell junctions in embryonic rat ventricular myocytes (ERVM), and their co-distribution is regulated by Ca^{2+}. Phosphoproteomics analysis revealed that obscurin-kin1 phosphorylates N-cadherin at Ser-788 located within the juxtamembrane region of its cytoplasmic domain with an apparent Kcat of ~5.05 min^{-1}. Overexpression of obscurin-kin1 or phosphomimic-Ser-788-Glu N-cadherin in ERVM markedly increases cell adhesion and chemical coupling. Importantly, phosphomimic-Ser-788-Glu N-cadherin exhibits significantly reduced binding to p120-catenin, while overexpression of phosphoablated-Ser-788-Ala N-cadherin increases RhoA activity. Consistent with an essential role of the obscurin-kin1/N-cadherin axis in cardiomyocyte coupling, it is deregulated in end-stage human heart failure. Given the nearly ubiquitous expression of obscurin and N-cadherin, our findings may have broad applicability in deciphering the obscurin-kin1/N-cadherin axis that likely mediates cell coupling in diverse tissues and organs.

Essential role of obscurin kinase-1 in cardiomyocyte coupling via N-cadherin phosphorylation

Li Wang[1*], Panagiotis Tsakiroglou[1*], Rex Gonzales[1*], Suhan Cho[1], Amy Li[2,3,4], Cristobal dos Remedios[5], Nathan Wright[6], and Aikaterini Kontrogianni-Konstantopoulos[1,#]

[1]*Department of Biochemistry and Molecular Biology, University of Maryland School of Medicine, Baltimore, MD 21201*

[2]*Sydney Heart Bank, The University of Sydney, Australia*

[3]*Department of Rural Clinical Sciences, La Trobe University, Bendigo VIC Australia 3550*

[4]*Centre for Healthy Futures, Torrens University, Pyrmont NSW Australia 20094*

[2,5]*Department of Mechanosensory Biology, Victor Chang Cardiac Research Institute, Darlinghurst NSW Australia 2010*

[6]*Department of Chemistry and Biochemistry, James Madison University, Harrisonburg, VA 22807*

*: Equally contributing authors

#: Correspondence to: Aikaterini Kontrogianni-Konstantopoulos, PhD
Phone#: 410-706-5788
Fax#: 410-706-8297

E-mail: akontrogianni@som.umaryland.edu

Conflict of Interest Statement: The authors have declared no conflict of interest exists.

Abstract

Obscurins are giant cytoskeletal proteins with structural and regulatory roles. Obscurin-B (~870 kDa), the largest known isoform, contains two enzymatically active Ser/Thr kinase (kin) domains, kin1 and kin2, which belong to the myosin light chain kinase (MLCK) family. Kin1 binds to and phosphorylates N-cadherin, a major component of the intercalated disc (ICD), the unique sarcolemmal microdomain that mediates the mechanochemical coupling of adjacent cardiomyocytes. Obscurin-B containing kin1 and N-cadherin co-localize at cell junctions in embryonic rat ventricular myocytes (ERVM), and their co-distribution is regulated by Ca^{2+}. Phosphoproteomics analysis revealed that obscurin-kin1 phosphorylates N-cadherin at Ser-788 located within the juxtamembrane region of its cytoplasmic domain with an apparent Kcat of ~5.05 min^{-1}. Overexpression of obscurin-kin1 or phosphomimic-Ser-788-Glu N-cadherin in ERVM markedly increases cell adhesion and chemical coupling. Importantly, phosphomimic-Ser-788-Glu N-cadherin exhibits significantly reduced binding to p120-catenin, while overexpression of phosphoablated-Ser-788-Ala N-cadherin increases RhoA activity. Consistent with an essential role of the obscurin-kin1/N-cadherin axis in cardiomyocyte coupling, it is deregulated in end-stage human heart failure. Given the nearly ubiquitous expression of obscurin and N-cadherin, our findings may have broad applicability in deciphering the obscurin-kin1/N-cadherin axis that likely mediates cell coupling in diverse tissues and organs.

Introduction

Obscurins encoded by the *OBSCN* gene comprise a family of giant cytoskeletal regulators exhibiting a nearly ubiquitous expression (1), with the highest prevalence in striated muscles (2, 3), where they play key roles in the organization of thick filaments, the sarcomeric alignment of internal membranes, the maintenance of the subsarcolemmal microtubule network, the modulation of RhoA and PI3K axes, and more recently the regulation of Ca^{2+} cycling (4-18). Consistent with the diverse roles of obscurins in muscle cells, missense, nonsense and frameshift mutations in *OBSCN* have been linked to different forms of cardiac and skeletal myopathies (19).

The prototypical obscurin, referred to as obscurin-A (~720 kDa), is composed of tandem immunoglobulin (Ig) and fibronectin-III (FnIII) domains followed by a cluster of signaling domains arranged in tandem and a non-modular COOH-terminus that contains ankyrin binding sites (3, 20, 21). Obscurin-B (~870 kDa), the largest known obscurin isoform, shares the same modular architecture with obscurin-A with the exception of its COOH-terminus that contains two Ser/Thr kinase domains, kin1 and kin2, that belong to the myosin light chain kinase (MLCK) subfamily (22, 23). Although the obscurin kinase domains have been identified for two decades, their enzymatic activity, regulation, substrates, and roles have remained enigmatic and at times controversial. Our group demonstrated that both kin1 and kin2 are enzymatically active, and that kin1 binds to and phosphorylates the cytoplasmic domain of N-cadherin *in vitro* (24).

N-cadherin is a Ca^{2+}-dependent transmembrane protein that is the principal component of adherens junctions (AJ) present at the intercalated disc (ICD), the unique sarcolemmal microdomain found at the bipolar ends of cardiomyocytes that mediates their mechanochemical

coupling (25, 26). N-cadherin is the only classical type-I cadherin expressed in the ICD , where it has a dual role; through its extracellular portion it connects adjoining cardiomyocytes in a homophilic way, while through its cytoplasmic portion it interacts with intracellular adaptor proteins, including a set of catenins and catenin-related proteins, linking the underlying cytoskeleton to the cell membrane (25, 27). The pivotal role of N-cadherin in maintaining cardiac structure and function has been demonstrated in several studies. As such, constitutive loss of N-cadherin in early development results in embryonic lethality, due to severe cardiovascular defects (28). Conversely, cardiac-specific loss of N-cadherin during adulthood leads to disassembly of the ICD, myofibrillar disarray, and dilated cardiomyopathy accompanied by ventricular arrhythmia and eventually sudden cardiac death (29-31).

To date, the molecular mechanisms that regulate the functional properties of N-cadherin have only been cursorily examined. Accordingly, Lee *et al.* demonstrated that N-cadherin is a target of endogenous kinases and phosphatases, and that its phosphorylation state is an important determinant of its stability and functionality at the cell surface (32). The same authors also reported that native N-cadherin contains high basal levels of Ser phosphorylation in the heart, retina, brain, and lens, while upon stimulation it undergoes further Ser and Tyr phosphorylation (32). Along these lines, Qi *et al.* documented that phosphorylation of N-cadherin by Src-kinase on Tyr-860 abolishes its ability to bind β-catenin at the plasma membrane of melanoma cells (33). Thus, phosphorylation of the cytoplasmic domain of N-cadherin is a potent mechanism that may regulate its stability, targeting, binding interactions, and mechanical/adhesive properties.

Herein we expand the roles of *OBSCN* in cell adhesion by showing that obscurin-kin1 is essential in the mechanochemical coupling of cardiomyocytes via phosphorylation of the cytoplasmic domain of N-cadherin at Ser-788. Our studies are of high pathophysiological relevance as they unravel a previously unknown molecular mechanism contributing to the regulation of cardiomyocyte adhesion and communication, which is deregulated in heart failure. Given the nearly ubiquitous expression of obscurins and N-cadherin, our findings may have broad applicability in characterizing a new regulatory axis that likely mediates cell coupling in diverse tissues and organs.

Results

Ca^{2+} regulated distribution of obscurin-kin1 and N-cadherin at cell junctions

Prior work from our group demonstrated that obscurin-kin1 specifically binds to and phosphorylates the cytoplasmic domain of N-cadherin *in vitro* (24). This finding was further supported by the coincident distribution of obscurin-B containing kin1 and N-cadherin at cell junctions in the ICD of adult cardiomyocytes (24). Given that the membrane targeting of N-cadherin is Ca^{2+} dependent (34), we performed Ca^{2+} switch experiments to examine if the preferential distribution of obscurin-B containing kin1 and N-cadherin at cell junctions is coordinately regulated by Ca^{2+}. We found that endogenous obscurin-B containing kin1 and N-cadherin co-distributed at cell junctions in both embryonic rat ventricular myocytes (ERVM; **Fig. 1A)** and HEK293 cells **(Fig. 1D)**, when grown in the presence of standard culture medium containing 1.8 mM $CaCl_2$. Removal of Ca^{2+} for 4 hr resulted in loss of both obscurin-B and N-cadherin from cell junctions, with residual proteins assuming a punctate and diffuse distribution in ERVM **(Fig. 1B)** and HEK293 cells **(Fig. 1E)**, respectively. Importantly, addition of 1.8 mM $CaCl_2$ in the culture medium resulted in redistribution of obscurin-B and N-cadherin to cell junctions in both ERVM **(Fig. 1C)** and HEK293 cells **(Fig. 1F)** within 1 hr.

Similar to endogenous obscurin-B, ectopically expressed GFP-tagged obscurin-kin1 containing the catalytic domain (GFP-Kin1-CA), but not control GFP-protein, targeted to the cell membrane in ERVM with a preferential accumulation at cell junctions where it colocalized with endogenous N-cadherin **(Fig. 1G)**, consistent with their direct association (24). In addition to its membrane localization, GFP-Kin1-CA also exhibited a punctate distribution in the cytoplasm. The co-distribution of exogenous GFP-Kin1-CA and endogenous N-cadherin at the cell membrane was

further confirmed by subcellular fractionation of HEK293 cells where ~36% of exogenous GFP-Kin1-CA was found in the membrane fraction, where endogenous N-cadherin was also detected **(Fig. 1H)**. Taken together, these findings support the coordinated, Ca^{2+}-dependent co-distribution of obscurin-B containing kin1 and N-cadherin at cell junctions, implying a (patho)physiological relevance of their association.

Obscurin-kin1 regulates cardiomyocyte adhesion and communication

Given the association and co-regulated distribution of obscurin-B containing kin1 and N-cadherin at cell junctions, we next investigated the role of kin1 in mediating cardiomyocyte adhesion and communication. To this end, we introduced control GFP and GFP-Kin1-CA in ERVM cultures and following cell sorting via flow cytometry we collected and assayed the GFP-positive cell populations. We first performed a dispase mechanical dissociation assay to examine the impact of GFP-Kin1-CA in modulating cardiomyocyte adhesion. ERVM expressing GFP-Kin1-CA exhibited a significantly lower number of cell fragments compared to ERVM expressing control GFP **(Fig. 2A)**, indicating that overexpression of GFP-Kin1-CA strengthens intercellular adhesion. Next, we investigated the effect of GFP-Kin1-CA in regulating intercellular communication via a dye transfer assay. Donor ERVM expressing GFP or GFP-Kin1-CA were labeled with the gap junction (GJ) transferable dye calcein deep red acetate, while recipient ERVM expressing GFP or GFP-Kin1-CA were labeled with the GJ non-transferable dye CytoTell red 590. ERVM expressing GFP-Kin1-CA displayed significantly increased rate of calcein deep red acetate dye transfer compared to ERVM expressing control GFP, following mixing of the respective donor and recipient cell populations **(Fig. 2B)**, suggesting that overexpression of GFP-Kin1-CA enhances GJ-mediated cell communication. Taken together, these results implicate obscurin-kin1

in the modulation of cardiomyocyte mechanochemical coupling, likely by directly regulating the phosphorylation status of N-cadherin and therefore its adhesive and mechanical properties.

Obscurin kinase 1 phosphorylates N-cadherin at Ser788.

To test our hypothesis that obscurin-kin1 modulates the mechanochemical coupling of cardiomyocytes via phosphorylation of N-cadherin, we set forth to identify the potential phosphorylation target site(s) of obscurin-kin1 within the cytoplasmic domain of N-cadherin. To this end, we used the baculovirus system to produce kin1-CA coupled to 6xHis-tag (His-Kin1-CA; **Supplemental Fig. 1A**) and the bacterial system to produce two different N-cadherin constructs tagged to 6xHis containing either the entire cytoplasmic domain (aa 746-906; accession no. P15116; His-Ncad$_{746-906}$, **Supplemental Fig. 1A)**, which we previously identified as the binding site of obscurin-kin1, or a smaller portion within the cytoplasmic domain (aa 786-880, accession no. P15116; His-Ncad$_{786-880}$, **Supplemental Fig. 1A**) that is enriched in Ser residues, which are predicted to be potential phosphorylation target sites by EXPASY/GPS2.1. Following affinity purification, His-Ncad$_{746-906}$ and His-Ncad$_{786-880}$ were subjected to *in vitro* kinase assays in the presence of His-Kin1-CA or control baculovirus preparation infected with empty vector that had undergone the same purification process as His-Kin1-CA. The reaction mixtures were subsequently subjected to liquid chromatography tandem mass spectrometry (LC-MS/MS) analysis. An N-cadherin peptide encompassing amino acids 786-808 containing a single phosphorylation event at Ser-788 was repeatedly identified in both the His-Ncad$_{746-906}$ **(Supplemental Fig. 1B)** and the His-Ncad$_{786-880}$ **(Supplemental Fig. 1C)** reaction mixtures when treated with His-Kin1-CA, but not with the control preparation. Sequence alignment using the Clustal Omega software indicated that Ser-788 is highly conserved among N-cadherin orthologs

across various species as well as among different members of the cadherin superfamily **(Supplemental Fig. 1D)**, suggesting that the identified phosphorylation event is of potential (patho)physiological relevance across different organisms and possibly within the cadherin superfamily.

To investigate the kinetics of the His-Kin1-CA/N-cadherin-Ser-788 phosphorylation reaction, we used a fluorometric assay to assess the apparent K_M and Vmax. We evaluated the His-Kin1-CA enzyme kinetics by varying the concentration of recombinant GST-Ncad$_{746-906}$ (substrate-1) between 70-2272 nM and maintaining the amount of ATP (substrate-2) constant at 100 μM. Our analysis yielded an apparent K_M of 232.8 nM and a Vmax of 2.63 x 10^{-3} nmoles ADP/min resulting in a Kcat of 5.05 min^{-1}, indicative of an efficient phosphorylation reaction **(Fig. 3A);** of note, similar catalytic turnover rates were independently obtained in parallel experiments **(Supplemental Fig. 2).** Importantly, use of control GST-protein or phosphoablated GST-Ncad$_{746-906}$ in which Ser-788 was replaced by Ala showed lack of phosphorylation of either recombinant protein by His-Kin1-CA **(Fig. 3A** and **Supplemental Fig. 2)**, further supporting the specificity of our findings.

To confirm the presence of phosphorylation on Ser-788 *in situ*, we generated phospho-specific antibodies, which we tested in immunoblots of protein lysates prepared from rat embryonic day 21 and adult hearts. We detected baseline phosphorylation of Ser-788 in both embryonic and adult cardiac lysates (**Fig. 3B)**, albeit to different extents, with the latter exhibiting ~2-fold lower levels, suggesting that Ser-788 phosphorylation may play a more potent role during embryonic heart development. Using immunofluorescence combined with confocal optics, we

further confirmed the presence of phospho-Ser-788 N-cadherin at cell junctions in developing ERVM **(Fig. 3C)** and the ICD in adult myocardium **(Fig. 3D)**.

Given the earlier observations by Lee *et al.* indicating that N-cadherin undergoes further phosphorylation upon stimulation (32), we next investigated if phosphorylation of Ser-788 responds to growth stimulation. We therefore treated ERVM cultures with 10 nM insulin and examined the effects of this treatment at regular intervals over a period of 360 min. We observed a statistically significant increase (~2-fold) in the levels of Ser-788 phosphorylation 10 min post-treatment compared to control (0 min), which gradually returned to basal levels (**Fig. 3E**), indicating that the obscurin-kin1/N-cadherin-Ser-788 phosphorylation axis may be modulated by responses elicited through activation of the insulin receptor, that plays a key role in the regulation of cardiac growth, survival, and metabolism (35).

N-cadherin phosphorylation on Ser-788 modulates cardiomyocyte adhesion and communication

We next investigated whether the effects of obscurin kin1-CA overexpression in the mechanochemical properties of cardiomyocytes are mediated through N-cadherin phosphorylation at Ser-788. To this end, we generated GFP-tagged wild type, phosphomimic and phosphoablated full-length N-cadherin constructs, referred to as GFP-N-cad-WT, GFP-N-cad-SE in which Ser-788 was substituted with glutamic acid (Glu, E), and GFP-N-cad-SA in which Ser-788 was substituted with alanine (Ala, A), respectively. Following transfection of these constructs in ERVM, GFP-positive cells were collected via cell sorting and subsequently subjected to dispase mechanical dissociation (**Fig. 4 A-B**) and dye transfer assay (**Fig. 4C**). Overexpression of GFP-N-cad-SE resulted in significantly decreased cell fragmentation (**Fig. 4 A-B**) and increased rate of

dye transfer following mixing of the respective donor and recipient cell populations (**Fig. 4C**), compared to control GFP and GFP-N-cad-SA, indicating that phosphorylation of N-cadherin at Ser-788 enhances cardiomyocyte adhesion and communication. Notably, similarly to GFP-N-cad-SE, overexpression of GFP-N-cad-WT resulted in a clear trend towards reduced cell fragmentation (**Fig. 4 A-B**) and significantly increased rate of dye transfer **(Fig. 4C)**, compared to control GFP and GFP-N-cad-SA, suggesting that exogenous GFP-N-cad-WT is likely phosphorylated by endogenous kin1 present in obscurin-B in ERVM.

Together these findings demonstrate that overexpression of obscurin-Kin1-CA **(Fig. 2)** and phosphomimic N-cadherin **(Fig. 4)** elicit the same responses on cardiomyocyte adhesion and communication. This strongly suggests that obscurin-kin1 modulates the mechanochemical properties of cardiomyocytes through phosphorylation of N-cadherin on Ser-788 located in the juxtamembrane region of its cytoplasmic domain.

N-cadherin phosphorylation at Ser-788 modulates binding to p120-catenin

Intracellularly, N-cadherin links the underlying actin cytoskeleton to the cell membrane via its direct and indirect interactions with a group of adaptor proteins, called catenins (25). P120-catenin binds to the juxtamembrane region (aa 774 – aa 790) of N-cadherin containing Ser-788 (36). We therefore examined if phosphorylation of N-cadherin at Ser-788 regulates their direct binding using GST-pull down assays. To this end, equivalent amounts of GST-tagged wild type (GST-Ncad$_{746-906}$-WT), phosphomimic (GST-Ncad$_{746-906}$-SE) and phosphoablated (GST-Ncad$_{746-906}$-SA) recombinant proteins containing the cytoplasmic domain of N-cadherin along with control GST were immobilized on a glutathione sepharose column via their GST-tag and incubated with

protein lysates prepared from adult mouse left ventricles **(Fig. 5A)**. GST-Ncad$_{746-906}$-SE exhibited significantly reduced binding to endogenous p120-catenin compared to GST-Ncad$_{746-906}$-WT and GST-Ncad$_{746-906}$-SA **(Fig. 5A)**, implicating Ser-788 phosphorylation in the regulation of the N-cadherin/p120-catenin binding. The specificity of this finding was corroborated by the lack of an effect in the binding of β-catenin to GST-Ncad$_{746-906}$-SE (**Fig. 5A**), which binds to the extreme COOH-terminus of N-cadherin (aa 856 – aa 885) (37).

To quantitatively evaluate the effect of Ser-788 phosphorylation on the N-cad/p120-catenin binding, we performed isothermal calorimetry (ITC) assays. GST-Ncad$_{746-906}$-WT and GST-Ncad$_{746-906}$-SE served as ligands while the middle portion of p120-catenin containing armadillo domains 1-8 (p120-catenin$_{311-747}$) that have been previously implicated in cadherin binding (38), fused to Maltose Binding Protein (MBP; **Fig. 5B)** served as sample macromolecule. An average binding affinity, K_D, of 1.25 $\pm$ 0.03 μM was determined for the GST-Ncad$_{746-906}$-WT and p120-catenin$_{311-747}$ proteins indicative of a moderate and dynamic interaction **(Fig. 5B)**. Remarkably, binding between GST-Ncad$_{746-906}$-SE and p120-catenin$_{311-747}$ was dramatically weaker with an average K_D of 196.85 $\pm$ 29.53 μM **(Fig. 5B)**, corroborating with the significantly reduced binding seen in the GST-pull down assay **(Fig. 5A)**.

Molecular dynamics simulation of phosphorylation of N-cadherin at Ser-788 and impact on RhoA activity

Earlier work has demonstrated that p120-catenin binding to cadherins modulates their targeting and stability to cell junctions and therefore their adhesive properties (36). In particular, p120-catenin binding has been implicated in preventing clathrin-mediated endocytosis of

cadherins and thus degradation via the lysosomal pathway (39). This process has been suggested to be mediated via a highly conserved acidic cluster of amino acid residues (i.e., DEE, aa 774-776 in N-cadherin) present in the core of the p120-catenin binding site on cadherins that functions as an endocytic signal when exposed, due to reduced binding of p120-catenin (40).

To explore how phosphorylation of N-cadherin at Ser-788 and ultimately the addition of a negative charge by the phosphate group affects the conformation of the N-cadherin/p120-catenin complex and thus the "exposure" of the DEE motif, we performed molecular dynamics simulations using phosphomimic-SE **(Fig. 6)** or phospho-Ser-788 **(Supplemental Fig. 3)** N-cadherin based on a model of the existing high resolution human E-cadherin/p120-catenin complex (PDB:3L6X) **(Fig. 6A)**. Of note, the relevant E- and N-cadherin peptides (carrying the p120-catenin binding site) are similar in sequence, with the only changes involving residues Phe-785 and His-791 which are replaced by Tyr and Gln in N-cadherin, respectively. Given that both substitutions are solvent-facing in the N-cadherin/p120 complex structure, they do not significantly alter any binding interactions upon model equilibration. Analysis of our models indicated that the NH_2-terminal region of the N-cadherin peptide binds p120-catenin through a series of electrostatic interactions, as described in (41). These remained unperturbed between the WT and phosphomimic-SE or phospho-Ser-788 N-cadherin/p120-catenin simulations. Conversely, the COOH-terminus of the N-cadherin peptides binds to p120-catenin primarily through hydrophobic interactions, made possible by N-cadherin residues 786-790 adopting a short 3-10 helix **(Fig. 6B)**. This helix is stabilized internally by several side-chain hydrogen bonds, including residues Asp-786 and Ser-788, Asp-786 and Gln-789, and Ser-788 and Gln-789. In the WT simulation, these interactions were present 96%, 42%, and 52% of the time, respectively. In contrast, in the SE-phosphomimic

(Fig. 6C) and phospho-Ser-788 **(Supplemental Fig. 3A)** simulations, these bonds were present 0%, 15%, and 8% and 4%, 0%, and 14% of the time, respectively. This loss of stabilizing interactions results in increased mobility in this 3-10 helix; this is evidenced by the SE-phosphomimic and phospho-Ser-788 N-cadherin variants having a larger root mean squared deviation (ΔRMSD=0.31 Å for phosphomimic-SE and ΔRMSD=0.13 Å for phospho-Ser-788) in this area compared to WT, with no concomitant ΔRMSD change in the rest of the peptide (**Fig. 6D** and **Supplemental Fig. 3B)**. This suggests that adding a negative charge to residue Ser-788 (via phosphorylation) destabilizes the binding-competent conformation of N-cadherin to p120-catenin, consistent with the reduction in p120-catenin affinity determined by the pull-down assays and ITC **(Fig. 5).** Interestingly though, the addition of a negative charge on Ser-788 fails to expose the "DEE" endocytic signature motif, implying that phosphorylation of N-cadherin at Ser-788 by obscurin-kin1 does not modulate its stability at the plasma membrane. In agreement with these findings, overexpression of GFP-tagged full length WT (GFP-Ncad-WT), SE phosphomimic (GFP-Ncad-SE) or SA phosphoablated (GFP-Ncad-SA) N-cadherin proteins in HEK293 cells indicated that they were expressed at similar levels **(Supplemental Fig. 4A),** and preferentially concentrated at the plasma membrane contrary to control GFP-protein which accumulated in the nucleus and perinuclear region, likely due to its small size **(Supplemental Fig. 4 B-E).**

Previous work has indicated that in addition to regulating cadherin stability at the plasma membrane, p120-catenin modulates the activity of small GTPases; in particular, it inhibits RhoA activity, which has been implicated in cadherin clustering, an early event in the assembly of cell junctions, and actin remodeling (39). Accordingly, it has been proposed that the ability of p120-catenin to modulate Rho GTPase activity may be inhibited by cadherin binding (39). We therefore

examined whether reduced binding of phosphorylated N-cadherin at Ser-788 to p120-catenin may affect RhoA activity. To this end, we used the HEK293 cells to overexpress GFP-tagged full length WT, phosphomimic-SE, and phosphoablated-SA N-cadherin proteins along with control GFP and performed GLiza assays to evaluate RhoA activity levels. Interestingly, while the expression levels of total RhoA were unaltered across control and experimental groups **(Fig. 6E)**, we found that RhoA activity was significantly increased following overexpression of phosphoablated-SA N-cadherin compared to control GFP protein and phosphomimic-SE N-cadherin **(Fig. 6F),** implicating Ser-788 phosphorylation in the regulation of RhoA-mediated processes via the dynamic binding of p120-catenin to N-cadherin and RhoA. Notably, overexpression of phosphomimic-SE N-cadherin did not induce a further decline in RhoA activity relative to control GFP, in agreement with the inherently low levels of endogenous RhoA **(**www.proteinatlas.org**)**, and therefore activity, in HEK293 cells. Moreover, WT N-cadherin behaved similarly to phosphoablated-SA N-cadherin exhibiting increased RhoA activity compared to control GFP and phosphomimic-SE N-cadherin, consistent with the relatively low levels of endogenous obscurin in HEK293 cells **(**www.proteinatlas.org**)**, implying lack of substantial phosphorylation of exogenous WT N-cadherin by endogenous obscurin-kin1.

Upregulation of the obscurin-B/N-cadherin phosphorylation axis in heart failure

Given the documented involvement of the *OBSCN* gene in the development of cardiomyopathies (19), we next interrogated whether the expression levels of obscurin-B containing kin1 and phospho-Ser-788 N-cadherin are altered in human end-stage heart failure DCM samples **(Table 1)**. Of note, the expression profile of obscurin-B in cardiac muscle has been controversial, with early reports suggesting that it is primarily expressed in skeletal muscles and

to a lesser extent in cardiac muscle, which was postulated to mainly contain small obscurin-kinase isoforms (22). To address this issue and given that most studies have used rodent myocardia, we performed RT-PCR analysis using human donor Left Ventricle (LV) samples as well as mouse myocardia to specifically amplify giant obscurin-B. Our findings indicated that contrary to mouse myocardia that contain minute amounts of obscurin-B transcripts **(Supplemental Fig. 5)** and protein under normal conditions (4, 11, 17), human donor LVs express adequate amounts of obscurin-B transcripts **(Supplemental Fig. 5)**, consistent with earlier studies reporting that obscurin-B appears to be the predominant isoform in human heart (42, 43). We therefore set forth to examine if the levels of obscurin-B containing kin1 and phospho-S788 N-cadherin were altered in human DCM end-stage heart failure LV samples compared to donor controls using antibodies to obscurin-kin1 as well as to phospho-Ser-788 and total N-cadherin **(Fig. 7)**. Importantly, we observed a significant increase in both the levels of obscurin-B containing kin1 and phospho-Ser-788 N-cadherin in DCM samples relative to controls, indicating that the obscurin-kin1/phospho-S788 N-cadherin axis is upregulated in human end-stage heart failure.

Discussion

Obscurins comprise a family of giant cytoskeletal regulators that are abundantly expressed in striated muscle cells, localizing in diverse subcellular compartments (2, 3). Obscurin-kinase isoforms preferentially accumulate at the ICD in adult cardiac muscle (24), the unique microdomain of the sarcolemma that contributes to the mechanochemical coupling of adjacent cardiomyocytes (26). Consistent with this, earlier work from our group indicated that obscurin-kin1 specifically binds to and phosphorylates the cytoplasmic domain of N-cadherin *in vitro* (24). N-cadherin is a major component of AJ mediating not only mechanical adhesion, but also contributing to the electrical coupling of adjoining cardiomyocytes and partaking in the organization of the cortical cytoskeleton through its interactions with a group of accessory proteins, collectively known as catenins (29, 44). Consistent with this, cardiac-specific loss of N-cadherin during adulthood leads to disassembly of the ICD, myofibrillar disarray, and dilated cardiomyopathy accompanied by ventricular arrhythmia and eventually sudden cardiac death (29).

Our current studies demonstrate that obscurin-B containing kin1 and N-cadherin co-distribute at contact sites in developing cardiomyocytes and their co-distribution is modulated by Ca^{2+}, highlighting the physiological relevance of the obscurin-kin1 regulation of N-cadherin. Accordingly, our mass spectrometry studies identified Ser-788, located in the juxtamembrane region of the cytoplasmic domain of N-cadherin, as the target-site of obscurin-kin1. Of note, smaller obscurin-kinase isoforms containing either both kin1 and kin2 (double kinase) or only kin2 (single kinase) have been described (22, 45), however their exact molecular identity and spatiotemporal distribution have remained elusive. Interestingly, Hsu *et al.,* reported phosphorylation of N-cadherin at Ser-788 in mouse embryonic fibroblasts in response to insulin

treatment in a comprehensive phosphoproteomics analysis, yet without identifying the responsible kinase or the physiological significance of this modification (46).

Twelve Ser/Thr kinases have been reported to modulate phosphorylation of AJ proteins, with all of them residing in the cytoplasm, that are likely recruited to AJ upon activation (47). Contrary to the identified cytoplasmic Ser/Thr kinases, which are suggested to transiently localize to AJ, a population of obscurin-B molecules containing kin1 appear to be permanently found at the ICD of cardiomyocytes. Although the activation mechanism of obscurin-kin1 is currently unknown, our studies showed that treatment of embryonic cardiomyocytes with insulin results in a rapid, transient upregulation of Ser-788 phosphorylation. Interestingly, bioinformatics analysis (PhosphoSitePlus) predicted the presence of phosphorylation within the catalytic portion of kin1, which is in agreement with its ability to undergo autophosphorylation *in vitro* (24). Moreover, Fleming *et al.*, reported that the linker region between kin1 and kin2 may contain several phosphorylation sites with at least some of them being (direct) targets of kin1, suggesting that such events may modulate kin1 (and possibly kin2) activity (48). In support of these observations, obscurin was recently identified as a kinase-bearing cytoskeletal protein to undergo extensive phosphorylation in response to exercise and maximal-intensity contractions in striated muscles, implicating it in hypertrophic and mechanotransduction responses (49, 50). Consistent with the notion that (auto)phosphorylation may play a key role in kin1's regulation, the NH_2-terminal Ser/Thr kinase domain (SK1) of *Striated muscle Preferentially Expressed Gene (SPEG),* which arose from *OBSCN* via gene duplication (23), is capable of autophosphorylation, while PKB/AKT directly phosphorylates the interkinase region of SPEG in response to insulin treatment, resulting in activation of the COOH-terminal SPEG kinase, SK2 (51). Although it is currently unknown

whether the enzymatic activity of obscurin-kin1 is also regulated by PKB/AKT, our earlier studies have shown that obscurin is intimately associated with the PI3K-PKB/AKT-mTOR pathway in both cardiomyocytes (4) and epithelial cells (13), and alteration of their association has major effects in key cellular processes including growth, adhesion, and motility/contractility.

Ectopic expression of catalytically active obscurin-kin1 in embryonic ventricular cardiomyocytes resulted in enhanced cell adhesion and communication. Although it is likely that obscurin-kin1 has additional targets in cardiomyocytes (24), it is reasonable to assume that the effects of kin1 in the modulation of the mechanochemical coupling of cardiomyocytes are mediated (at least in part) via phosphorylation of N-cadherin at Ser-788. In accordance with this, overexpression of phosphomimic N-cadherin in embryonic cardiomyocytes elicited similar effects. Notably, baseline phosphorylation of Ser-788 was considerably higher in embryonic compared to adult cardiomyocytes, suggesting that it may have a more prominent role during cardiac development and differentiation when cell junction assembly takes place (39), rather than in adulthood where intercellular connections have already formed.

The molecular mechanisms that regulate the functional properties of N-cadherin have only been cursorily examined. Accordingly, Lee *et al* demonstrated that N-cadherin is a target of endogenous kinases and phosphatases, and that its phosphorylation state is an important determinant of its stability and functionality at the cell surface (32). Moreover, the same authors reported that native N-cadherin contains high basal levels of Ser phosphorylation in the heart, retina, brain, and lens, whereas upon stimulation it undergoes further Ser and Tyr phosphorylation (32). Consistent with this, Qi *et al.* documented that phosphorylation of N-cadherin by Src-kinase

on Tyr-860 abolishes its ability to bind β-catenin at the plasma membrane of melanoma cells, inhibiting their transmigration across the endothelium (33), while Tyr phosphorylation of N-cadherin promotes its proteolytic cleavage and diminishes cell adhesion (32). While the extracellular domain of N-cadherin mediates cell adhesion in a homophilic way in a Ca^{2+}-dependent manner, its cytoplasmic domain is also involved in the construction of tight and compact cell junctions by supporting interactions with the underlying actin cytoskeleton (52, 53). Such binding interactions involve the formation of a dynamic multi-protein complex consisting of linker proteins (e.g. catenins), GTPases (e.g. RhoA), ubiquitin ligases (e.g. Hakai ligase), kinases (e.g. PIPKIγ and obscurin-kin1 as our data indicate), and phosphatases (e.g. PTPσ) (54, 55).

Previous work has demonstrated that p120-catenin binds to the juxtamembrane region (aa774-aa790) of N-cadherin (39) that contains Ser-788. This region of N-cadherin, which is normally disordered, is anchored to p120-catenin via electrostatic interactions involving the Asp774-Glu775-Glu776 (DEE) motif and hydrophobic interactions encompassing residues Leu-787, Ser-788, Gln-789 and Leu-790 (41). Asp-774 and Leu-790 are separated by more than 3 nm in the N-cadherin-bound p120-catenin form, and there is no obvious mechanism through which phosphorylation of Ser-788 would directly influence the structure, dynamics, and binding capacity of the DEE motif. Instead, Ser-788 phosphorylation disrupts the local N-cadherin secondary structure. This in turn appears to destabilize the hydrophobic interactions between the juxtamembrane region of N-cadherin and p120-catenin, likely leading to peeling away of N-cadherin from the p120-catenin binding groove, consistent with our *in vitro* binding studies, without exposing the DEE endocytic signal (40, 56). Thus, it appears that obscurin-kin1 mediated

phosphorylation of N-cadherin at Ser-788, that results in reduced binding to p120-catenin, is not involved in N-cadherin internalization and degradation.

In addition to regulating the trafficking and stability of N-cadherin at the plasma membrane, cadherin-uncoupled, cytoplasmic p120-catenin potently inhibits RhoA activity, either directly via binding or indirectly via Rac1 activation, impacting its ability to modulate the (re)organization of the cortical cytoskeleton (39, 57, 58). Importantly, the dynamic binding of p120-catenin to cadherins appears to be regulated via phosphorylation (59). Consistent with this, phosphorylation of E-cadherin at Tyr-755/756 or VE-cadherin at Tyr-658 disrupts p120-catenin binding. We therefore postulate that obscurin-kin1 mediated phosphorylation of N-cadherin at Ser-788 results in reduced N-cadherin/p120-catenin binding, which in turn frees up p120-catenin to negatively regulate RhoA activity. This notion would be consistent with elevated RhoA activity in the absence of N-cadherin phosphorylation at Ser-788, which is in agreement with our findings following overexpression of phosphoablated N-cadherin. More importantly, in accordance with our studies indicating enhanced mechanochemical coupling of embryonic cardiomyocytes following overexpression of obscurin-kin1 or phosphomimic N-cadherin, reduced RhoA activity has been implicated in promoting cell adhesion (39, 58, 60).

Given the reported involvement of the *OBSCN* gene in different forms of cardiomyopathies (19) along with the elevation of obscurins in preclinical models of myocardial hypertrophy and ventricular tachycardia (17, 61, 62), our findings demonstrating upregulation of the obscurin-B/phospho-N-cadherin axis in end-stage DCM may be of high pathophysiological relevance. As such, it is plausible that upregulation of the obscurin-B/phospho-N-cadherin axis may underlie

enhanced mechanical coupling and thus elevated stiffness consistent with the DCM pathology as well as increased electrical coupling leading to changes in cardiomyocyte conductance and development of arrhythmia. Consistent with this, 7 out of the 9 DCM patients that we evaluated presented with atrial fibrillation while 2 also exhibited ventricular tachycardia **(Table 1)**. It is important to note that of the ~20 known *OBSCN* variants linked to the development of heart disease, 3 immediately flank kin1 and are associated with the development of LVNC or DCM, while 1 resides within the kin1 catalytic domain, possibly affecting its enzymatic activity and/or substrate specificity and is associated with the development of DCM.

Taken together, our studies uncover a previously unknown axis mediating cardiomyocyte coupling that involves the regulation of N-cadherin via obscurin-kin1 mediated phosphorylation at Ser-788. Given the nearly ubiquitous expression of both obscurin and N-cadherin, our findings may have broad applicability and impact in identifying and characterizing this new signaling axis that may contribute to the regulation of cell coupling in diverse tissues and organs.

Methods

Primary Antibodies

All primary antibodies used in the study are included in Supplemental Information.

Expression constructs and recombinant proteins

A description of the source or generation of constructs and recombinant proteins is provided in Supplemental Information.

Preparation and culturing of embryonic rat ventricular myocytes (ERVM)

ERVM were isolated from hearts of embryonic day 21 (E21) Sprague-Dawley rats, as previously described (4). A description of the procedure is included in Supplemental Information.

Ca^{2+} switch assay

ERVM and HEK293 cells were plated on laminin (20 μg/ml) coated coverslips and cultured overnight in DMEM-F12 media containing 5% FBS, 100 U/ml penicillin-streptomycin and DMEM media containing 10% FBS, 100 U/ml penicillin-streptomycin, respectively, in the presence of 1.8 mM $CaCl_2$ (Thermo Fisher Scientific) to allow cell attachment before switching to medium lacking Ca^{2+}. Following incubation for 4 hr in Ca^{2+} depleted media, cells were switched back to Ca^{2+} containing media for 1 hr, and subsequently processed for immunofluorescent staining (please see below) followed by confocal imaging.

Transfection of ERVM followed by immunofluorescent staining and confocal evaluation

ERVM were plated on laminin (20 μg/ml) coated coverslips and allowed to adhere overnight before they were transfected with 1 μg/μl of control pEGFPN1 or pEGFPN1-Kin1-CA plasmids using the TransIT-LT1 transfection reagent (Mirus Bio LLC, Madison, WI) according to the manufacturer's instructions. 72 hr post-transfection, ERVM cultures were fixed with ice-cold 100% methanol for 30 min at -20°C, permeabilized with 0.1% Triton X-100 for 5 min, blocked with 5% goat serum for 1 hr, and incubated with the indicated primary antibodies overnight at 4°C. Following extensive washes with PBS, samples were incubated with the appropriate secondary antibodies conjugated with Alexa Fluor dyes (Thermo Fisher Scientific) for 1 hr at room temperature and mounted with Prolong antifade mounting medium (Thermo Fisher Scientific). Samples were imaged under confocal optics (Zeiss LSM510 META NLO or LSM DUO) with an X63 objective.

Transfection of HEK293 cells and cell fractionation

HEK293 cells were plated on 6-well plates and following establishment of a confluent monolayer they were transfected with 2.5 μg of control pEGFPN1 or pEGFPN1-Kin1-CA plasmid using Lipofectamine^{TM}3000 (Thermo Fisher Scientific). Cell fractionation was performed 72 hr post-transfection using the MEM-PER plus membrane protein extraction kit (Thermo Fisher Scientific) to separate the membrane and cytosolic fractions, as described by the manufacturer. Equivalent amounts of cytosolic and membrane protein fractions were separated by Novex® NuPAGE SDS-PAGE (Thermo Fisher Scientific), transferred to nitrocellulose membrane, and probed with the indicated primary antibodies followed by the appropriate horse radish peroxidase (HRP)-conjugated secondary antibodies (i.e., goat anti-rabbit IgG; Cat #: 7074, 1:3,000 dilution,

Cell Signaling Technology). Immunoreactive bands were visualized with SignalFire ECL reagent (Cell Signaling Technology) in an Amersham Imager 680 (Amersham Biosciences).

Dispase assay

ERVM cultures were transiently transfected as described above with the following plasmids: pEGFP-N1, pEGFP-N1-Kin1-CA, pEGFP-N1-N-cadherin-WT, pEGFP-N1-N-cadherin-S788E, and pEGFP-N1-N-cadherin-S788A. Seventy-two hr post-transfection, ERVM were sorted for GFP fluorescence via flow cytometry (BD FACSAria II; BD Biosciences). GFP-positive cells were re-plated in a 48-well plate pre-coated with Geltrex (0.035 mg/ml, Life Technologies), and subjected to dispase assay, as in (4); a description of the dispase assay is included in Supplemental Information.

Dye transfer assay

ERVM cultures transfected with pEGFP-N1, pEGFP-N1-Kin1-CA, pEGFP-N1-N-cadherin-WT, pEGFP-N1-N-cadherin-S788E, and pEGFP-N1-N-cadherin-S788A were subjected to dye transfer assays, as in (63, 64) with minor modifications; a description is provided in Supplemental Information.

Expression and purification of His-tagged obscurin kinase-1 from insect cells

A detailed description of the expression and purification of His-tagged obscurin kinase-1 is provided in Supplemental Information.

In vitro kinase assay and tandem mass spectrometry

1 μg of 6xHis-Kin1-CA purified protein or negative control was incubated with 1 μg of His-Ncad$_{746-906}$ including the cytoplasmic domain of N-cadherin or His-Ncad$_{786-880}$ including part of the cytoplasmic domain of N-cadherin enriched in potential Ser/Thr phospho-sites, in kinase buffer containing 10 mM Na_2HPO_4, 10 mM $MgCl_2$, 200 μM ATP, 1 mM $CaCl_2$, 1 mM DTT, and 100 nM okadaic acid, in the presence of Halt protease and phosphatase inhibitors (Thermo Scientific) at 4°C overnight. The reaction mixtures were subsequently subjected to tandem mass spectrometry (Johns Hopkins School of Medicine, Mass Spectrometry Core) to examine the presence of phosphorylation site(s). A description of the tandem mass spectrometry is included in Supplemental Information. Phospho-S788 was identified one and six times in His-Ncad$_{746-906}$ and His-Ncad$_{786-880}$, respectively, with 100% probability. Data are available via ProteomeXchange with identifier PXD031003.

Determination of Vmax, K_M and Kcat of the obscurin-kin1/N-cadherin-S788 phosphorylation reaction

The Universal fluorometric nonradioactive assay kit (ab138879, Abcam) was used to detect and measure the *in vitro* kinase activity of His-Kin1-CA. Briefly, the activity of His-Kin1-CA was assessed by measuring ADP formation, which is directly proportional to the enzyme's phosphotransferase activity. Fluorescence intensity was measured at varying substrate concentrations (70-2900 nM) with a fluorescent plate reader (Synergy HTX, BioTek) at excitation/emission 540/590 nm. Substrates, including GST-Ncad$_{746-906}$-WT, GST-Ncad$_{746-906}$-SA, and GST, were incubated with a constant amount of His-Kin1-CA, set at 26 nM, and 100 μM of ATP in a 96-well plate in the dark for 1hr at 25 °C. At the end of the incubation period, 20 μl of

ADP sensor buffer and 10 µl of fluorescent ADP sensor were added to each reaction. Relative Fluorescence Units (RFU) at each substrate concentration were measured in duplicate and converted to total nanomoles of ADP produced using an ADP standard curve. The amount of ADP formed per min at each substrate concentration was calculated by dividing the total nanomoles of ADP formed by the reaction time (i.e., 60 min). Nanomoles of ADP formed per min from n=3 independent experiments performed in duplicate were fitted using GraphPad Prism nonlinear regression software for Michaelis Menten kinetics to calculate the apparent Vmax and Km, while the apparent Kcat was obtained by dividing the fitted Vmax by the total nanomoles of the enzyme. The three experiments are independently presented in **Fig. 3A** and **Supplemental Fig. 2** (instead of being averaged), due to the generation and use of different standard curves; all three experiments yielded similar catalytic turnover rates.

Preparation of protein lysates from embryonic and adult rat hearts

E21 and 3-month old adult rat hearts were harvested and homogenized in ice-cold lysis buffer containing 10 mM Na_3PO_4 (pH 7.2), 2 mM EDTA, 10 mM NaN_3, 120 mM NaCl, and 1% NP40 supplemented with Halt protease and phosphatase inhibitors (Thermo Fisher Scientific), using a microbeads homogenizer (TissueLyser LT, Hilden, Germany). Following tissue homogenization, samples were incubated at 4 °C for ~60 min using gentle rotation prior to centrifugation at 12,000 rpm at 4 °C for 20 min. Protein concentration was determined using the bicinchoninic acid (BCA) protein assay (BCA protein assay kit, ThermoFisher Scientific). Twenty µg of protein lysates from embryonic and adult hearts were separated by Novex® NuPAGE SDS-PAGE (Thermo Fisher Scientific, Rockford, IL), transferred to nitrocellulose membrane, and probed with the indicated primary antibodies followed by the appropriate HRP-conjugated

secondary antibodies (i.e., goat anti-rabbit IgG; Cat #: 7074,1:3,000 dilution, Cell Signaling Technology).

Immunofluorescence staining of ERVM cultures and adult mouse hearts

ERVM isolated from n=12 E21 Sprague Dawley rats were plated on ibidi-coated 96-well plates (μ-Plate 96-Well Black; ibidi GmbH, Germany) and allowed to adhere overnight. Three days post-plating, ERVM cultures were fixed with 4% paraformaldehyde (PFA) in PBS for 30 min, permeabilized with 0.1% Triton X-100 for 10 min, blocked with 1 mg/ml BSA, 1mM NaN_3, 50 mM glycine in PBS for 1 hr, and incubated with N-Cad-pS788 (20 μg/ml) and "total" N-cadherin (3B9, dilution 1:200, Thermofisher) antibodies. Three adult mice (1-, 3-, and 6-month old) were perfused with 4% PFA under anesthesia. Hearts were excised and embedded in OCT Embedding Compound (Tissue-Tek, Sakura, Torrance, CA) and gradually frozen using 2-methylbutane at -60°C. Cardiac sections (~10 μm) were obtained with a Micron HM550 cryostat (Thermo Scientific), permeabilized with 0.1% Triton X-100 for 25 min, blocked with 1 mg/ml BSA, 1 mM NaN_3, 50 mM glycine in PBS for 1 hr, and incubated overnight with N-Cad-pS788 (40 μg/ml) and "total" N-cadherin (3B9, dilution 1:200, Thermofisher) antibodies. Following extensive washes with PBS, ERVM cultures and adult cardiac sections were incubated with the appropriate secondary antibodies conjugated to Alexa Fluor-488 and Alexa Flour-647 for 2 hr at room temperature and then counterstained with 1:400 Hoechst (Invitrogen). Adult cardiac sections were mounted with ProLong Diamond Antifade Mountant (Invitrogen). Specimens were analyzed under a Nikon Eclipse Ti2 spinning disk confocal microscope equipped with a 60x, 1.49 numerical aperture oil immersion TIRF objective using dual laser settings at 525 nm and 665 emission wavelengths with 500 ms and 200 ms exposure time, respectively.

Insulin treatment of ERVM cultures

ERVM cultures were serum-starved overnight prior to treatment with 10 nM insulin (Sigma-Aldrich, St. Louis, MO; cat # 10516) for the indicated time points (i.e., 0, 10, 30, 60, 180 and 30 min), subsequently washed with ice-cold PBS (2x), and harvested in ice-cold lysis buffer containing 10 mM Na_3PO_4 (pH 7.2), 2 mM EDTA, 10 mM NaN_3, 120 mM NaCl, and 1% NP40 supplemented with Halt protease and phosphatase inhibitors (Thermo Fisher Scientific, Rockford, IL). Following incubation on ice for 60 min and gentle pipetting, cell lysates were obtained by centrifugation at 12,000 rpm at 4 °C for 20 min. 30 μg of protein lysates from each time point were evaluated via immunoblotting using the indicated primary antibodies followed by the appropriate alkaline phosphatase (AP)-conjugated secondary antibodies (i.e., goat anti-mouse IgG, 1:3,000 dilution, cat #: A3688, Sigma-Aldrich and goat anti-rabbit IgG, 1: 3,000 dilution, cat # AB_2337947, Jackson Immunoresearch), while immunoreactive bands were visualized by chemiluminescence (NovaBright, Thermo Fisher Scientific).

GST-pull down assays

Equivalent amounts of GST, GST-$Ncad_{746-906}$-WT, GST-$Ncad_{746-906}$-S788E, and GST-$Ncad_{746-906}$-S788A were immobilized on glutathione sepharose beads via their GST-tag and incubated with 1 mg of 3-month old adult mouse heart lysates prepared in lysis buffer containing 10 mM Na_3PO_4, pH 7.2, 10 mM NaN_3, 120 mM NaCl, 1 mM $CaCl_2$, and 1% NP40 supplemented with a cOmplete^{TM} protease inhibitor tablet (Roche Applied Science, Mannheim, Germany) at 4°C overnight. Following extensive washes with lysis buffer, complexes were eluted with 2X SDS loading buffer, boiled for 10 min, resolved by SDS-PAGE, and analyzed via immunoblotting using the indicated primary antibodies followed by the appropriate alkaline phosphatase (AP)-

conjugated secondary antibodies (i.e., goat anti-mouse IgG, 1:3,000 dilution, cat # A3688, Sigma-Aldrich and goat anti-rabbit IgG, 1:3,000, cat # AB_2337947, Jackson Immunoresearch). Immunoreactive bands were visualized by chemiluminescence (NovaBright, Thermo Fisher Scientific). Binding of p120-catenin or β-catenin to GST-Ncad$_{746-906}$-S788E and GST-Ncad$_{746-906}$-S788A is expressed relatively to GST-Ncad$_{746-906}$-WT, which was arbitrarily set to 1.

Isothermal titration calorimetry (ITC)

The binding interaction of ligands GST-Ncad$_{476-906}$-WT and GST-Ncad$_{476-906}$-SE to sample macromolecule MBP-p120-catenin$_{311-747}$ was monitored using a VP-ITC titration microcalorimeter (MicroCal Inc., Northampton, MA) at 37°C. For all experiments, ligands and sample macromolecule were dialyzed into PBS pH 7.4 (Quality Biological^{tm}, Gaithersburg, MD), degassed under vacuum and equilibrated at 37°C prior to titration. Ligand solutions varied between 80-100 μM of total protein, while the ITC sample chamber (1.8 ml volume) contained 10 μM of MBP-P120-catenin$_{311-747}$. Three sets of control experiments were performed: in the first, 100 μM of each ligand was injected into PBS buffer; in the second, 100 μM of each ligand was injected into PBS containing 10 μM MBP; and in the third, 100 μM GST was titrated into PBS containing 10 μM MBP-p120-catenin$_{311-747}$. Heat change from control titrations was subtracted from experimental titrations. Three different recombinant protein preparations were used for each of the three experimental replicates with all showing similar results. Data were fit to a one-site binding model using Origin® (MicroCal) to obtain K_D values. The K_D values from all 3 experimental replicates were averaged and the SEM was calculated. The number of binding sites for GST-Ncad$_{476-906}$-SE titrations was manually fixed to 1 for model fitting due to the considerably weak interaction.

Computational modeling

Molecular dynamics simulations using the mouse N-cadherin/p120 complex model (based off the human E-cadherin/p120-catenin structure; pdb accession number 3L6X) were run on WT, the S787E phosphomimic variant and the phospho-S788 form of N-cadherin, introduced by the 'swap' command in YASARA (41, 65). These simulations were run at 310°K, 150 mM NaCl, pH 7.4 using the Amber ff14 forcefield in a simulation cell with periodic boundaries for 100 ns. Simulations were run with a time-step of 1.25 fs with the temperature adjusted using a Berendsen thermostat as described in (65). Both simulations stabilized within 5 ns at judged by RMSD, and analyses were performed in 100 ps intervals from 5-100 ns using YASARA macros.

Immunoblotting and immunofluorescence analysis of HEK293 cells ectopically expressing GFP-N-cadherin variants

HEK293 cells were plated on glass coverslips pre-coated with Geltrex (0.035 mg/ml, Life Technologies) in 35 mm dishes and allowed to reach 80-90% confluency at which time-point they were transfected with 1 μg/μl of control pEGFP-N1, pEGFP-N1-N-cadherin-WT, pEGFP-N1-N-cadherin-S788E, and pEGFP-N1-N-cadherin-S788A plasmids using the TransIT-LTI transfection reagent (Mirus Bio LLC). 48hr post-transfection, HEK293 cultures were either processed for immunoblotting or immunofluorescence analysis. Specifically, protein lysates were prepared using RIPA buffer (#89900, Thermo Fisher Scientific, USA) containing protease/phosphatase inhibitors (#78446, Thermo Fisher Scientific, USA). Immunoblotting was performed as described above, while detection of immunoreactive bands was performed with the ECL detection system (SignalFire ECL reagent, Cat# 6883, Cell Signaling Technology). Conversely, cells were fixed with ice-cold 100% methanol for 30 min at -20°C, permeabilized with 0.1% Triton X-100 for 5

min, blocked with 5% goat serum for 1 hr, and incubated with the indicated primary antibodies overnight at 4°C. Following extensive washes with PBS, samples were incubated with the appropriate secondary antibodies conjugated with Alexa Fluor dyes (Thermo Fisher Scientific) for 1 hr at room temperature and mounted with Prolong antifade mounting medium (Thermo Fisher Scientific). Samples were imaged under confocal optics (Zeiss LSM510 META NLO or LSM DUO) with an X63 objective.

RhoA activity measurements using G-LISA assay

The levels of active RhoA (GTP-RhoA) were evaluated using the G-LISA RhoA luminescence activation assay kit (#BK121, Cytoskeleton, Denver, CO) following the manufacturer's instructions. In brief, following lysis of HEK293 cells transfected with 1 μg/μl of control pEGFP-N1, pEGFP-N1-N-cadherin-WT, pEGFP-N1-N-cadherin-S788E, and pEGFP-N1-N-cadherin-S788A plasmids, 50 μl of each sample and the appropriate negative (blank) and positive controls were assayed in 96-well G-LISA plates, while the signal was measured using a microplate luminometer (Synergy, Agilent, USA). Moreover, the levels of total RhoA were evaluated via immunoblotting analysis as described above using 20 μg of protein lysates prepared in RIPA buffer (#89900, Thermo Fisher Scientific, USA) and the ECL detection system (SignalFire ECL reagent, Cat# 6883, Cell Signaling Technology).

RNA isolation and Reverse Transcription Polymerase Chain Reaction (RT-PCR)

A description of the RNA isolation method and the RT-PCR is provided in Supplemental Information.

Preparation of protein lysates from control and heart failure human samples

Human donor control and DCM heart failure samples were obtained from the Sydney Heart Bank, Australia in collaboration with St. Vincent's Hospital, Sydney. Human heart tissue used in this study was collected with the informed and written consent of transplant patients or from the families of organ donors of non-failing hearts in accordance with the principles in the Declaration of Helsinki. Ethical approval was provided by the Human Research Ethics Committees at the University of Sydney (2016/7326) and St Vincent's Hospital (H03/118). Material Transfer Agreement was executed between the University of Sydney and the University of Maryland Baltimore, School of Medicine (Ref: #CT14876). Samples included 9 end-stage DCM LVs consisting of 6 males and 3 females ranging in age between 31-64 years old, and 6 age-matched donor LVs consisting of 5 males and 1 female, ranging in age between 29-63 years old **(Table 1)**.

Protein lysates from control and heart failure LV samples were prepared as described in (17). In brief, samples were grinded to powder in liquid nitrogen with a mortar and pestle. The grinded tissue was kept at -20 °C for 20 minutes, followed by solubilization in lysis buffer containing 8 M urea, 2 M thiourea, 3% (w/v) sodium dodecyl sulfate (SDS), 0.05 M Tris-HCl (pH 6.8), 0.075 M dithiothreitol (DTT), 0.03% (w/v) bromophenol blue, and 10% (w/v) glycerol, supplemented with Halt protease and phosphatase inhibitors (Thermo Fisher Scientific) in a 60 °C water bath. Following centrifugation, aliquoted protein lysates were flash frozen in liquid nitrogen and immediately stored in -80 °C. Given that the presence of urea/thiourea does not allow determination of protein concentration, starting from equal amounts of control and experimental tissue enables equivalent loading among samples (17). Accordingly, equal volumes of control and heart failure protein lysates were heated at 55 °C for 5 min, separated by Novex® NuPAGE SDS-

PAGE (Thermo Fisher Scientific), transferred to nitrocellulose membrane, and probed with the indicated primary antibodies followed by the appropriate HRP-conjugated secondary antibody (i.e., goat anti-rabbit IgG; Cat#: 7074, 1:3000 dilution, Cell Signaling Technology). Immunoreactive bands were visualized by ECL chemiluminescence (SignalFire ECL reagent, Cat# 6883, Cell Signaling Technology).

Presentation of Coomassie Blue gels and immunoblots

All Coomassie Blue gels and immunoblots are shown in "greyscale" mode for consistency of presentation. Given the limited availability/amounts of some samples, horizontal strips from the same blot were cut across at the appropriate molecular weight and probed with the relevant antibodies to ensure that the expression levels of "proteins of interest" were evaluated in the same lysates.

Statistics

Statistical tests, sample numbers, number of biological/technical repeats and p-values are provided in figure legends; values are expressed as mean +/- SEM. Densitometric evaluation of immunoreactive bands was performed with Image J software.

Study Approval

All animal work was conducted under a protocol approved by the Institutional Animal Care and Use Committee (IACUC) of the University of Maryland School of Medicine. Human heart tissue was collected with the informed and written consent of transplant patients or from the

families of organ donors of non-failing hearts in accordance with the principles in the Declaration of Helsinki.

Data availability

Raw blots, gels, and images are included in the “Supporting Information” pptx file with areas shown in figures marked with white dashed or red solid boxes. In addition, values for all data points shown in graphs are included in the “Supporting Data Values” xls file.

Author contributions

LW: conceptualization, experimentation, validation, formal analysis, investigation, writing original draft, editing. **PT:** conceptualization, experimentation, validation, formal analysis, investigation, writing and editing. **RG**: conceptualization, experimentation, validation, formal analysis, investigation, writing and editing. **SC:** experimentation, validation, formal analysis, investigation, writing and editing. **AL:** resources and editing. **CDR:** resources and editing. **NTW:** modeling, formal analysis, investigation, validation, writing and editing, funding acquisition. **AKK:** conceptualization, writing and editing, supervision, project administration, funding acquisition.

Acknowledgements

The authors would like to thank Dr. Stephan Lange for insightful feedback and resources, Dr. Li-Yen R. Hu for thoughtful discussions, and Drs. David Weber and Brianna Young for permission to use the ITC instrument and for technical support during ITC experimentation.

This work was supported by the National Institutes of Health/National Institute of Arthritis, Musculoskeletal and Skin Diseases (NIH/NIAMS) Interdisciplinary Training Program in Muscle Biology T32 AR007592 to LW, PT and RG, the NIH/NIAMS R01AR077106 and NIH/NHLBI R01HL165634 to AKK, and the National Science Foundation RUI MCB-2024182 and Camille and Henry Dreyfus Foundation TH-18-019 to NTW.

References

1. Ackermann MA, Shriver M, Perry NA, Hu LY, and Kontrogianni-Konstantopoulos A. Obscurins: Goliaths and Davids take over non-muscle tissues. *PLoS One.* 2014;9(2):e88162.
2. Kontrogianni-Konstantopoulos A, Ackermann MA, Bowman AL, Yap SV, and Bloch RJ. Muscle giants: molecular scaffolds in sarcomerogenesis. *Physiol Rev.* 2009;89(4):1217-67.
3. Wang L, Geist J, Grogan A, Hu LR, and Kontrogianni-Konstantopoulos A. Thick Filament Protein Network, Functions, and Disease Association. *Compr Physiol.* 2018;8(2):631-709.
4. Ackermann MA, King B, Lieberman NAP, Bobbili PJ, Rudloff M, Berndsen CE, et al. Novel obscurins mediate cardiomyocyte adhesion and size via the PI3K/AKT/mTOR signaling pathway. *J Mol Cell Cardiol.* 2017;111:27-39.
5. Bagnato P, Barone V, Giacomello E, Rossi D, and Sorrentino V. Binding of an ankyrin-1 isoform to obscurin suggests a molecular link between the sarcoplasmic reticulum and myofibrils in striated muscles. *J Cell Biol.* 2003;160(2):245-53.
6. Borisov AB, Kontrogianni-Konstantopoulos A, Bloch RJ, Westfall MV, and Russell MW. Dynamics of obscurin localization during differentiation and remodeling of cardiac myocytes: obscurin as an integrator of myofibrillar structure. *J Histochem Cytochem.* 2004;52(9):1117-27.
7. Borisov AB, Sutter SB, Kontrogianni-Konstantopoulos A, Bloch RJ, Westfall MV, and Russell MW. Essential role of obscurin in cardiac myofibrillogenesis and hypertrophic response: evidence from small interfering RNA-mediated gene silencing. *Histochem Cell Biol.* 2006;125(3):227-38.
8. Ford-Speelman DL, Roche JA, Bowman AL, and Bloch RJ. The rho-guanine nucleotide exchange factor domain of obscurin activates rhoA signaling in skeletal muscle. *Mol Biol Cell.* 2009;20(17):3905-17.
9. Kontrogianni-Konstantopoulos A, Catino DH, Strong JC, Randall WR, and Bloch RJ. Obscurin regulates the organization of myosin into A bands. *Am J Physiol Cell Physiol.* 2004;287(1):C209-17.
10. Kontrogianni-Konstantopoulos A, Jones EM, Van Rossum DB, and Bloch RJ. Obscurin is a ligand for small ankyrin 1 in skeletal muscle. *Mol Biol Cell.* 2003;14(3):1138-48.
11. Lange S, Ouyang K, Meyer G, Cui L, Cheng H, Lieber RL, et al. Obscurin determines the architecture of the longitudinal sarcoplasmic reticulum. *J Cell Sci.* 2009;122(Pt 15):2640-50.
12. Raeker MO, Bieniek AN, Ryan AS, Tsai HJ, Zahn KM, and Russell MW. Targeted deletion of the zebrafish obscurin A RhoGEF domain affects heart, skeletal muscle and brain development. *Dev Biol.* 2010;337(2):432-43.
13. Shriver M, Marimuthu S, Paul C, Geist J, Seale T, Konstantopoulos K, et al. Giant obscurins regulate the PI3K cascade in breast epithelial cells via direct binding to the PI3K/p85 regulatory subunit. *Oncotarget.* 2016;7(29):45414-28.
14. Benian GM, Tinley TL, Tang X, and Borodovsky M. The Caenorhabditis elegans gene unc-89, required fpr muscle M-line assembly, encodes a giant modular protein composed of Ig and signal transduction domains. *J Cell Biol.* 1996;132(5):835-48.
15. Qadota H, Blangy A, Xiong G, and Benian GM. The DH-PH region of the giant protein UNC-89 activates RHO-1 GTPase in Caenorhabditis elegans body wall muscle. *J Mol Biol.* 2008;383(4):747-52.

16. Spooner PM, Bonner J, Maricq AV, Benian GM, and Norman KR. Large isoforms of UNC-89 (obscurin) are required for muscle cell architecture and optimal calcium release in Caenorhabditis elegans. *PLoS One.* 2012;7(7):e40182.
17. Grogan A, Coleman A, Joca H, Granzier H, Russel MW, Ward CW, et al. Deletion of obscurin immunoglobulin domains Ig58/59 leads to age-dependent cardiac remodeling and arrhythmia. *Basic Res Cardiol.* 2020;115(6):60.
18. Hu LR, Ackermann MA, Hecker PA, Prosser BL, King B, O'Connell KA, et al. Deregulated Ca(2+) cycling underlies the development of arrhythmia and heart disease due to mutant obscurin. *Sci Adv.* 2017;3(6):e1603081.
19. Grogan A, and Kontrogianni-Konstantopoulos A. Unraveling obscurins in heart disease. *Pflugers Arch.* 2019;471(5):735-43.
20. Busby B, Oashi T, Willis CD, Ackermann MA, Kontrogianni-Konstantopoulos A, Mackerell AD, Jr., et al. Electrostatic interactions mediate binding of obscurin to small ankyrin 1: biochemical and molecular modeling studies. *J Mol Biol.* 2011;408(2):321-34.
21. Busby B, Willis CD, Ackermann MA, Kontrogianni-Konstantopoulos A, and Bloch RJ. Characterization and comparison of two binding sites on obscurin for small ankyrin 1. *Biochemistry.* 2010;49(46):9948-56.
22. Russell MW, Raeker MO, Korytkowski KA, and Sonneman KJ. Identification, tissue expression and chromosomal localization of human Obscurin-MLCK, a member of the titin and Dbl families of myosin light chain kinases. *Gene.* 2002;282(1-2):237-46.
23. Grogan A, Tsakiroglou P, and Kontrogianni-Konstantopoulos A. Double the trouble: giant proteins with dual kinase activity in the heart. *Biophys Rev.* 2020;12(4):1019-29.
24. Hu LY, and Kontrogianni-Konstantopoulos A. The kinase domains of obscurin interact with intercellular adhesion proteins. *FASEB J.* 2013;27(5):2001-12.
25. Vite A, and Radice GL. N-cadherin/catenin complex as a master regulator of intercalated disc function. *Cell Commun Adhes.* 2014;21(3):169-79.
26. Pruna M, and Ehler E. The intercalated disc: a mechanosensing signalling node in cardiomyopathy. *Biophys Rev.* 2020;12(4):931-46.
27. Zuppinger C, Eppenberger-Eberhardt M, and Eppenberger HM. N-Cadherin: structure, function and importance in the formation of new intercalated disc-like cell contacts in cardiomyocytes. *Heart Fail Rev.* 2000;5(3):251-7.
28. Radice GL, Rayburn H, Matsunami H, Knudsen KA, Takeichi M, and Hynes RO. Developmental defects in mouse embryos lacking N-cadherin. *Dev Biol.* 1997;181(1):64-78.
29. Kostetskii I, Li J, Xiong Y, Zhou R, Ferrari VA, Patel VV, et al. Induced deletion of the N-cadherin gene in the heart leads to dissolution of the intercalated disc structure. *Circ Res.* 2005;96(3):346-54.
30. Li J, Levin MD, Xiong Y, Petrenko N, Patel VV, and Radice GL. N-cadherin haploinsufficiency affects cardiac gap junctions and arrhythmic susceptibility. *J Mol Cell Cardiol.* 2008;44(3):597-606.
31. Li J, Patel VV, Kostetskii I, Xiong Y, Chu AF, Jacobson JT, et al. Cardiac-specific loss of N-cadherin leads to alteration in connexins with conduction slowing and arrhythmogenesis. *Circ Res.* 2005;97(5):474-81.
32. Lee MM, Fink BD, and Grunwald GB. Evidence that tyrosine phosphorylation regulates N-cadherin turnover during retinal development. *Dev Genet.* 1997;20(3):224-34.

33. Qi J, Wang J, Romanyuk O, and Siu CH. Involvement of Src family kinases in N-cadherin phosphorylation and beta-catenin dissociation during transendothelial migration of melanoma cells. *Mol Biol Cell.* 2006;17(3):1261-72.
34. Volk T, and Geiger B. A 135-kd membrane protein of intercellular adherens junctions. *EMBO J.* 1984;3(10):2249-60.
35. Abel ED. Insulin signaling in the heart. *Am J Physiol Endocrinol Metab.* 2021;321(1):E130-E45.
36. Thoreson MA, Anastasiadis PZ, Daniel JM, Ireton RC, Wheelock MJ, Johnson KR, et al. Selective uncoupling of p120(ctn) from E-cadherin disrupts strong adhesion. *J Cell Biol.* 2000;148(1):189-202.
37. Mohamet L, Hawkins K, and Ward CM. Loss of function of e-cadherin in embryonic stem cells and the relevance to models of tumorigenesis. *J Oncol.* 2011;2011:352616.
38. Hong JY, Oh IH, and McCrea PD. Phosphorylation and isoform use in p120-catenin during development and tumorigenesis. *Biochim Biophys Acta.* 2016;1863(1):102-14.
39. Anastasiadis PZ. p120-ctn: A nexus for contextual signaling via Rho GTPases. *Biochim Biophys Acta.* 2007;1773(1):34-46.
40. Nanes BA, Chiasson-MacKenzie C, Lowery AM, Ishiyama N, Faundez V, Ikura M, et al. p120-catenin binding masks an endocytic signal conserved in classical cadherins. *J Cell Biol.* 2012;199(2):365-80.
41. Ishiyama N, Lee SH, Liu S, Li GY, Smith MJ, Reichardt LF, et al. Dynamic and static interactions between p120 catenin and E-cadherin regulate the stability of cell-cell adhesion. *Cell.* 2010;141(1):117-28.
42. Marston S. Obscurin variants and inherited cardiomyopathies. *Biophys Rev.* 2017;9(3):239-43.
43. Marston S, Montgiraud C, Munster AB, Copeland O, Choi O, Dos Remedios C, et al. OBSCN Mutations Associated with Dilated Cardiomyopathy and Haploinsufficiency. *PLoS One.* 2015;10(9):e0138568.
44. Radice GL. N-cadherin-mediated adhesion and signaling from development to disease: lessons from mice. *Prog Mol Biol Transl Sci.* 2013;116:263-89.
45. Borisov AB, Raeker MO, and Russell MW. Developmental expression and differential cellular localization of obscurin and obscurin-associated kinase in cardiac muscle cells. *J Cell Biochem.* 2008;103(5):1621-35.
46. Hsu PP, Kang SA, Rameseder J, Zhang Y, Ottina KA, Lim D, et al. The mTOR-regulated phosphoproteome reveals a mechanism of mTORC1-mediated inhibition of growth factor signaling. *Science.* 2011;332(6035):1317-22.
47. Bertocchi C, Vaman Rao M, and Zaidel-Bar R. Regulation of adherens junction dynamics by phosphorylation switches. *J Signal Transduct.* 2012;2012:125295.
48. Fleming JR, Rani A, Kraft J, Zenker S, Borgeson E, and Lange S. Exploring Obscurin and SPEG Kinase Biology. *J Clin Med.* 2021;10(5).
49. Guo H, Isserlin R, Emili A, and Burniston JG. Exercise-responsive phosphoproteins in the heart. *J Mol Cell Cardiol.* 2017;111:61-8.
50. Potts GK, McNally RM, Blanco R, You JS, Hebert AS, Westphall MS, et al. A map of the phosphoproteomic alterations that occur after a bout of maximal-intensity contractions. *J Physiol.* 2017;595(15):5209-26.

51. Quan C, Du Q, Li M, Wang R, Ouyang Q, Su S, et al. A PKB-SPEG signaling nexus links insulin resistance with diabetic cardiomyopathy by regulating calcium homeostasis. *Nat Commun.* 2020;11(1):2186.
52. Hong S, Troyanovsky RB, and Troyanovsky SM. Binding to F-actin guides cadherin cluster assembly, stability, and movement. *J Cell Biol.* 2013;201(1):131-43.
53. Perez-Moreno M, Jamora C, and Fuchs E. Sticky business: orchestrating cellular signals at adherens junctions. *Cell.* 2003;112(4):535-48.
54. Figueiredo J, Soderberg O, Simoes-Correia J, Grannas K, Suriano G, and Seruca R. The importance of E-cadherin binding partners to evaluate the pathogenicity of E-cadherin missense mutations associated to HDGC. *Eur J Hum Genet.* 2013;21(3):301-9.
55. Guo Z, Neilson LJ, Zhong H, Murray PS, Zanivan S, and Zaidel-Bar R. E-cadherin interactome complexity and robustness resolved by quantitative proteomics. *Sci Signal.* 2014;7(354):rs7.
56. Garrett JP, Lowery AM, Adam AP, Kowalczyk AP, and Vincent PA. Regulation of endothelial barrier function by p120-cateninVE-cadherin interaction. *Mol Biol Cell.* 2017;28(1):85-97.
57. Noren NK, Liu BP, Burridge K, and Kreft B. p120 catenin regulates the actin cytoskeleton via Rho family GTPases. *J Cell Biol.* 2000;150(3):567-80.
58. Anastasiadis PZ, Moon SY, Thoreson MA, Mariner DJ, Crawford HC, Zheng Y, et al. Inhibition of RhoA by p120 catenin. *Nat Cell Biol.* 2000;2(9):637-44.
59. Kourtidis A, Ngok SP, and Anastasiadis PZ. p120 catenin: an essential regulator of cadherin stability, adhesion-induced signaling, and cancer progression. *Prog Mol Biol Transl Sci.* 2013;116:409-32.
60. Wildenberg GA, Dohn MR, Carnahan RH, Davis MA, Lobdell NA, Settleman J, et al. p120-catenin and p190RhoGAP regulate cell-cell adhesion by coordinating antagonism between Rac and Rho. *Cell.* 2006;127(5):1027-39.
61. Borisov AB, Raeker MO, Kontrogianni-Konstantopoulos A, Yang K, Kurnit DM, Bloch RJ, et al. Rapid response of cardiac obscurin gene cluster to aortic stenosis: differential activation of Rho-GEF and MLCK and involvement in hypertrophic growth. *Biochem Biophys Res Commun.* 2003;310(3):910-8.
62. Wu Y, Bell SP, Trombitas K, Witt CC, Labeit S, LeWinter MM, et al. Changes in titin isoform expression in pacing-induced cardiac failure give rise to increased passive muscle stiffness. *Circulation.* 2002;106(11):1384-9.
63. Thompson SA, Blazeski A, Copeland CR, Cohen DM, Chen CS, Reich DM, et al. Acute slowing of cardiac conduction in response to myofibroblast coupling to cardiomyocytes through N-cadherin. *J Mol Cell Cardiol.* 2014;68:29-37.
64. Kizana E, Chang CY, Cingolani E, Ramirez-Correa GA, Sekar RB, Abraham MR, et al. Gene transfer of connexin43 mutants attenuates coupling in cardiomyocytes: novel basis for modulation of cardiac conduction by gene therapy. *Circ Res.* 2007;100(11):1597-604.
65. Krieger E, Darden T, Nabuurs SB, Finkelstein A, and Vriend G. Making optimal use of empirical energy functions: force-field parameterization in crystal space. *Proteins.* 2004;57(4):678-83.

Figures and Figure Legends

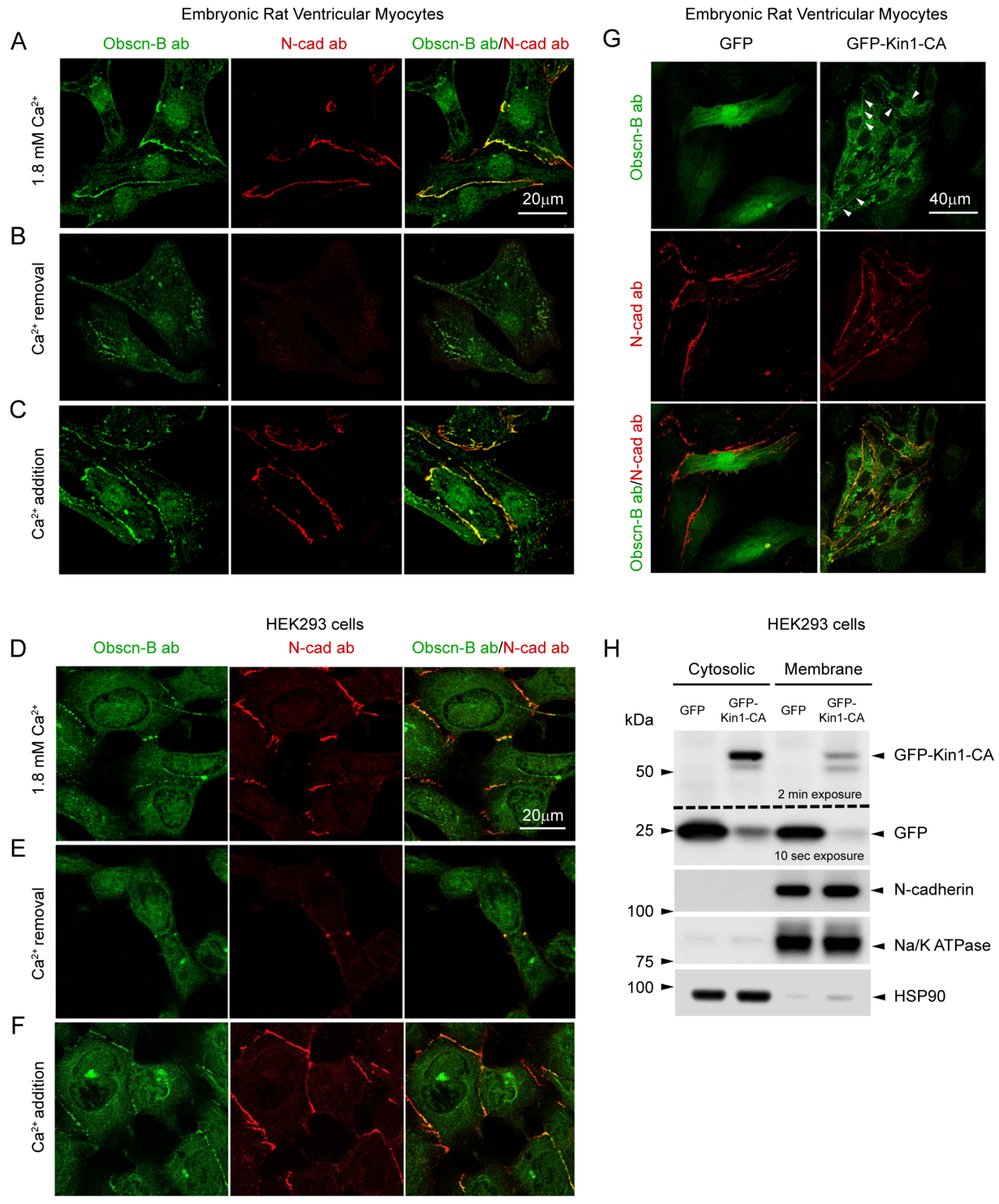

Figure 1: The co-distribution of obscurin-B containing kin1 and N-cadherin at cell junctions is coordinately regulated by Ca^{2+}. A-C and **D-F:** Ca^{2+} switch experiments combined with

confocal imaging demonstrated that obscurin-B co-localizes with N-cadherin at cell junctions in primary cultures of ERVM (A) and HEK293 cells (D) in the presence of Ca^{2+}. Ca^{2+} removal for 4 hr resulted in loss of both obscurin-B and N-cadherin from cell junctions, with residual proteins exhibiting a punctate or diffuse cytoplasmic distribution in ERVM (B) and HEK293 cells (E), respectively. Addition of Ca^{2+} in the medium for 1 hr restored the co-distribution of obscurin-B and N-cadherin at cell junctions in both ERVM (C) and HEK293 cells (F); n=4 experiments for ERVM (4 optical fields per condition, per experiment) and n=2 for HEK293 cells (5-6 optical fields per condition, per experiment). **G:** Confocal evaluation of ERVM cultures transfected with control GFP and GFP-Kin1-CA indicated that exogenous GFP-Kin1-CA, but not GFP-protein, co-localizes with endogenous N-cadherin at cell contact sites (arrowheads); n=3 experiments. **H:** Cell fractionation of HEK293 cells transfected with control-GFP or GFP-Kin1-CA followed by immunoblotting analysis showed that ~36% of exogenous GFP-Kin1-CA is found in the membrane fraction similarly to endogenous N-cadherin; the identity of the membrane and cytoplasmic fractions was confirmed by probing for Na/K ATPase and HSP90, respectively, which also served as loading controls within each fraction; n=3 experiments.

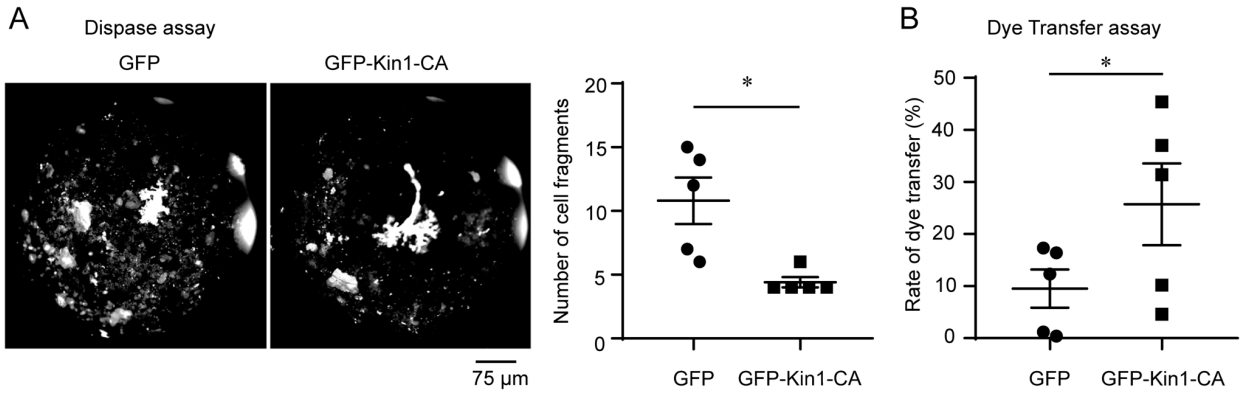

Figure 2: Obscurin-kin1 modulates cardiomyocyte mechanochemical coupling. Overexpression of GFP-Kin1-CA, but not control GFP-protein, in ERVM significantly increases cardiomyocyte adhesion as shown by the reduced number of cell fragments ($\geq$ 100 µm) obtained in a dispase assay (**A**; n=5, two-tailed paired t-test, p=0.0362), and intercellular communication as indicated by the increased rate of dye transfer (**B**; n=5, two-tailed paired t-test, p=0.0206). Data are expressed as mean $\pm$ SEM; * indicates statistical significance.

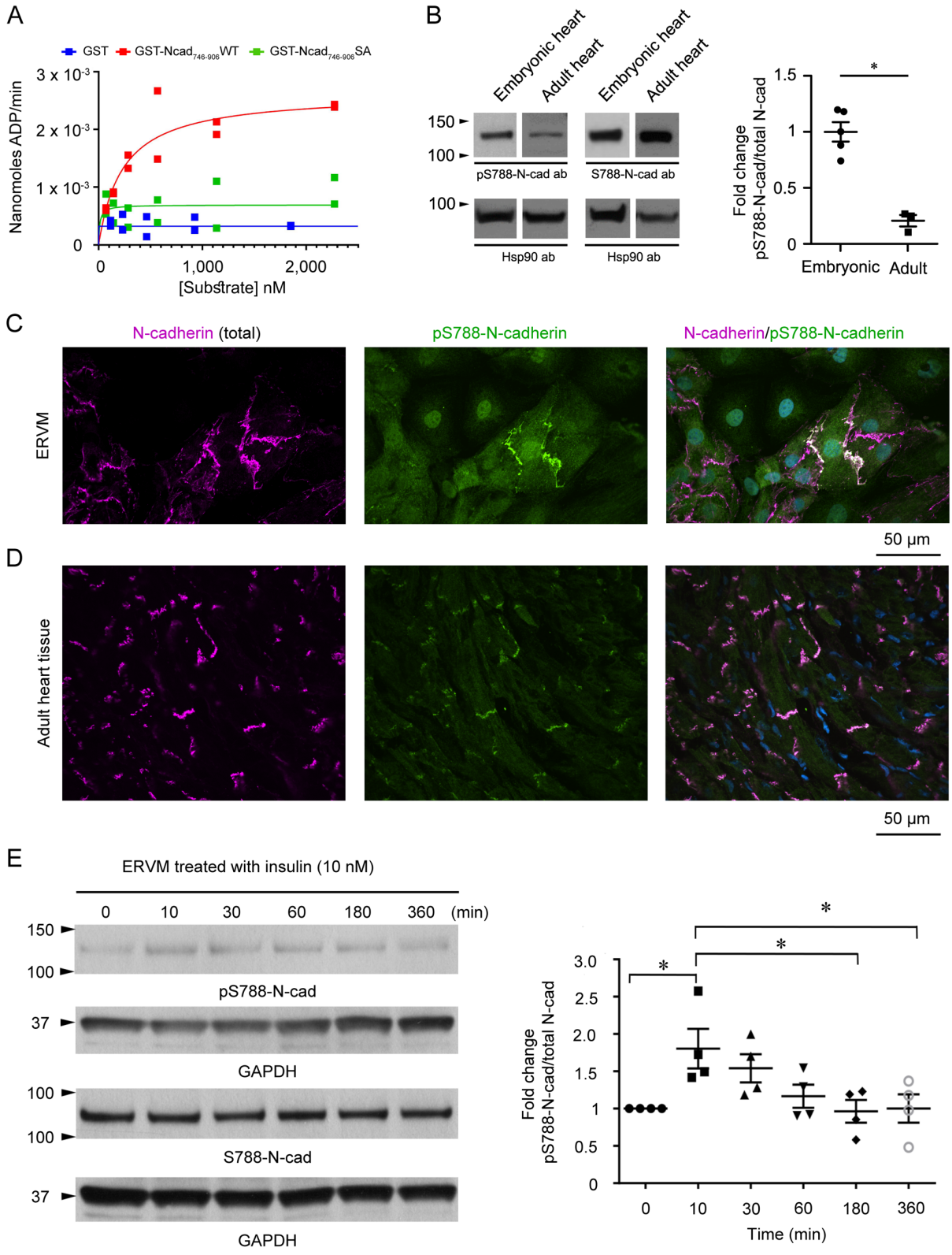
A
GST
GST-Ncad746-906WT
GST-Ncad746-906SA
Nanomoles ADP/min
3 x 10-3
2 x 10-3
1 x 10-3
0
0
1,000
2,000
[Substrate] nM
B
Embryonic heart
Adult heart
Embryonic heart
Adult heart
150
100
pS788-N-cad ab
S788-N-cad ab
100
Hsp90 ab
Hsp90 ab
Fold change pS788-N-cad/total N-cad
1.5
1
0.5
0
*
Embryonic
Adult
C
N-cadherin (total)
pS788-N-cadherin
N-cadherin/pS788-N-cadherin
ERVM
50 μm
D
Adult heart tissue
50 μm
E
ERVM treated with insulin (10 nM)
0
10
30
60
180
360
(min)
150
100
pS788-N-cad
37
GAPDH
100
100
S788-N-cad
37
GAPDH
Fold change pS788-N-cad/total N-cad
3.0
2.5
2.0
1.5
1
0.5
0
*
*
*
0
10
30
60
180
360
Time (min)

Figure 3: Obscurin kin1 phosphorylates N-cadherin at Ser-788. A: Michaelis-Menten plot showing the nmoles of ADP produced per min at constant amount of His-Kin1-CA (26 nM) and ATP (100 μM) and varying substrate concentrations (70-2272 nM). An apparent Vmax (2.63 x 10^{-3} nmoles ADP/min), K_M (232.8 nM), and Kcat (5.05 min^{-1}) for GST-$Ncad_{746-906}$-WT were calculated, while use of GST and GST-$Ncad_{746-906}$-SA did not yield any appreciable ADP formation. Data values from two technical repeats at each substrate concentration are shown. **B:** Representative immunoblots using custom-made affinity-purified phospho-Ser-788 N-cadherin (pS788-N-cad) and total Ser-788 (S788-N-cad) antibodies with protein lysates prepared from embryonic day-21 (E21) and adult (3-month old) rat hearts. Although baseline phosphorylation of N-cadherin at Ser-788 was observed in both embryonic and adult hearts, the former contain a 2-fold higher ratio of pS788-N-cad/total N-cad compared to the latter. Quantification was performed following normalization to Hsp90 that was used as loading control. Non-continuous lanes are separated with white space (please see Supporting Information); n=5 biological samples for embryonic rat hearts and n=3 biological samples for adult rat hearts run in duplicate; unpaired Mann Whitney two-tailed t-test, p=0.0357. **C-D:** Immunofluorescent staining of ERVM cultures (C) and 1-month old mouse myocardia (D) with phospho-Ser-788 and total N-cadherin antibodies followed by confocal evaluation showed the presence of phospho-Ser-788 N-cadherin at cell junctions and ICDs, respectively; ERVM cultures and tissue sections were counterstained with Hoechst to identify nuclei. **E:** Immunoblotting of ERVM protein lysates with pS788-N-cad and S788-N-cad antibodies following treatment with 10 nM insulin indicated a statistically significant increase in the phosphorylation levels of N-cadherin at Ser-788 at 10 min, which returned to pre-treatment levels by 180 min; quantification of the pS788-N-cad/total N-cad ratio at the indicated time points was performed following normalization to GAPDH that was used as loading control

with the pS788-N-cad/total N-cad ratio at 0 min set to 1 and ratios at remaining time points expressed relative to it; n=4, one-way ANOVA followed by Tukey's multiple comparisons test, p=0.0486 (10 min *vs* 0 min), p=0.0365 (10 min *vs* 180 min) and p=0.0491 (10 min *vs* 360 min). Data are expressed as mean ± SEM; *: indicates statistical significance.

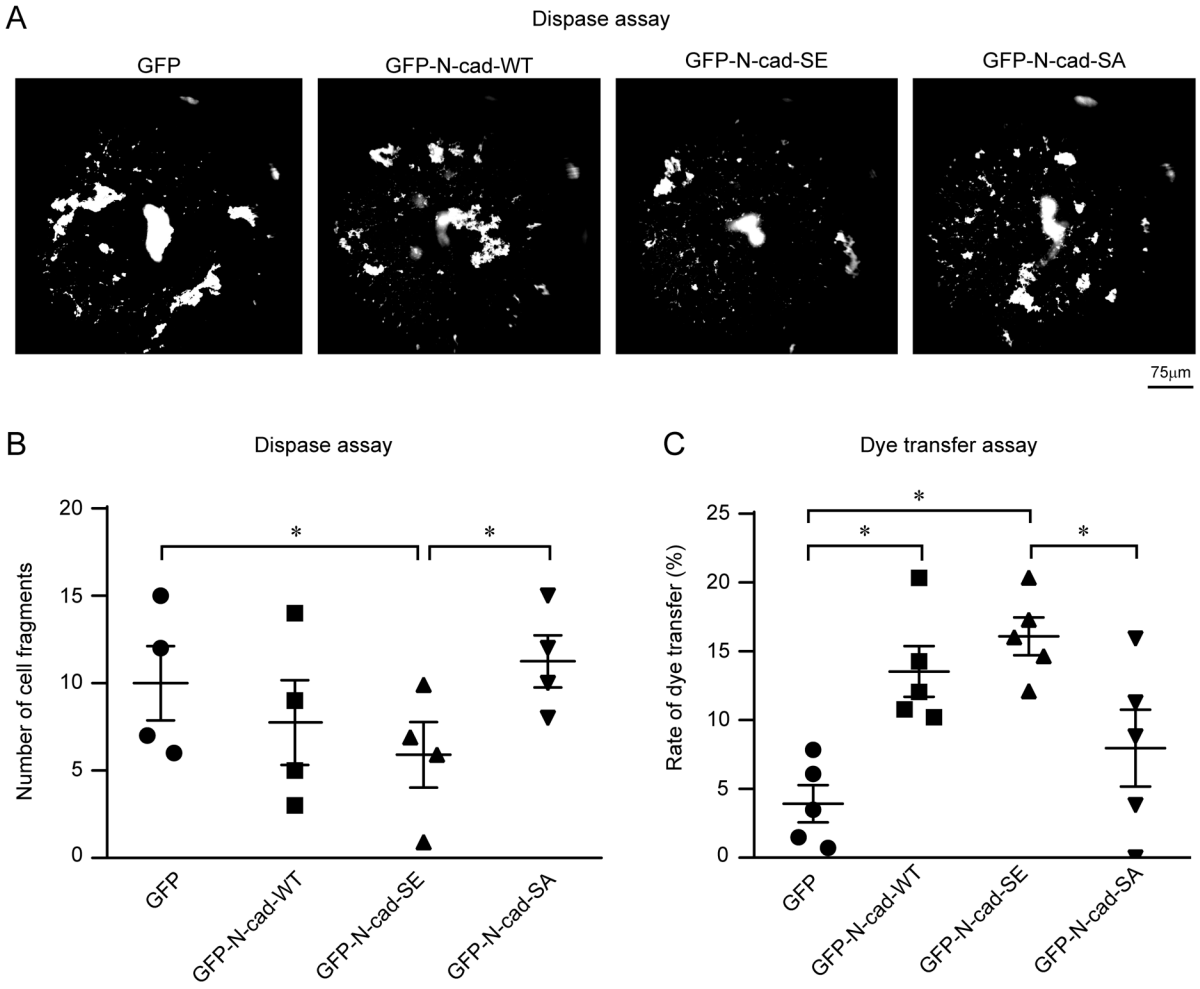

Figure 4: Phosphorylation of N-cadherin at Ser-788 plays a key role in cardiomyocyte adhesion and communication. A-B: Overexpression of phosphomimic GFP-N-cad-SE, but not control GFP-protein or phosphoablated GFP-N-cad-SA in ERVM significantly increased cardiomyocyte adhesion as indicated by the reduced number of cell fragments ($\geq$ 100 μm) obtained in a dispase assay; of note, wild type GFP-N-cad-WT shows a clear trend towards increased mechanical coupling; n=4, repeated measures one-way ANOVA followed by Fisher's Least Significant Difference (LSD) post-hoc test; p=0.028 for comparison of GFP-N-cad-SE *vs* GFP and p=0.0036 for comparison of GFP-N-cad-SE *vs* GFP-N-cad-SA. **C:** Overexpression of phosphomimic GFP-N-cad-SE, but not control GFP-protein or phosphoablated GFP-N-cad-SA, in

ERVM significantly enhances intercellular communication as shown by the increased rate of dye transfer; interestingly, overexpression of wild type GFP-N-cad-WT elicits the same effect suggesting that it may be phosphorylated by endogenous kin1present in obscurin-B (n=5, repeated measures one-way ANOVA followed by Tukey's multiple comparisons test, p=0.008 for comparison of GFP-N-cad-SE *vs* GFP, p=0.0386 for comparison of GFP-N-cad-SE *vs* GFP-N-cad-SA, and p=0.0023 for comparison of GFP-N-cad-WT *vs* GFP. Data are expressed as mean $\pm$ SEM; *: indicates statistical significance.

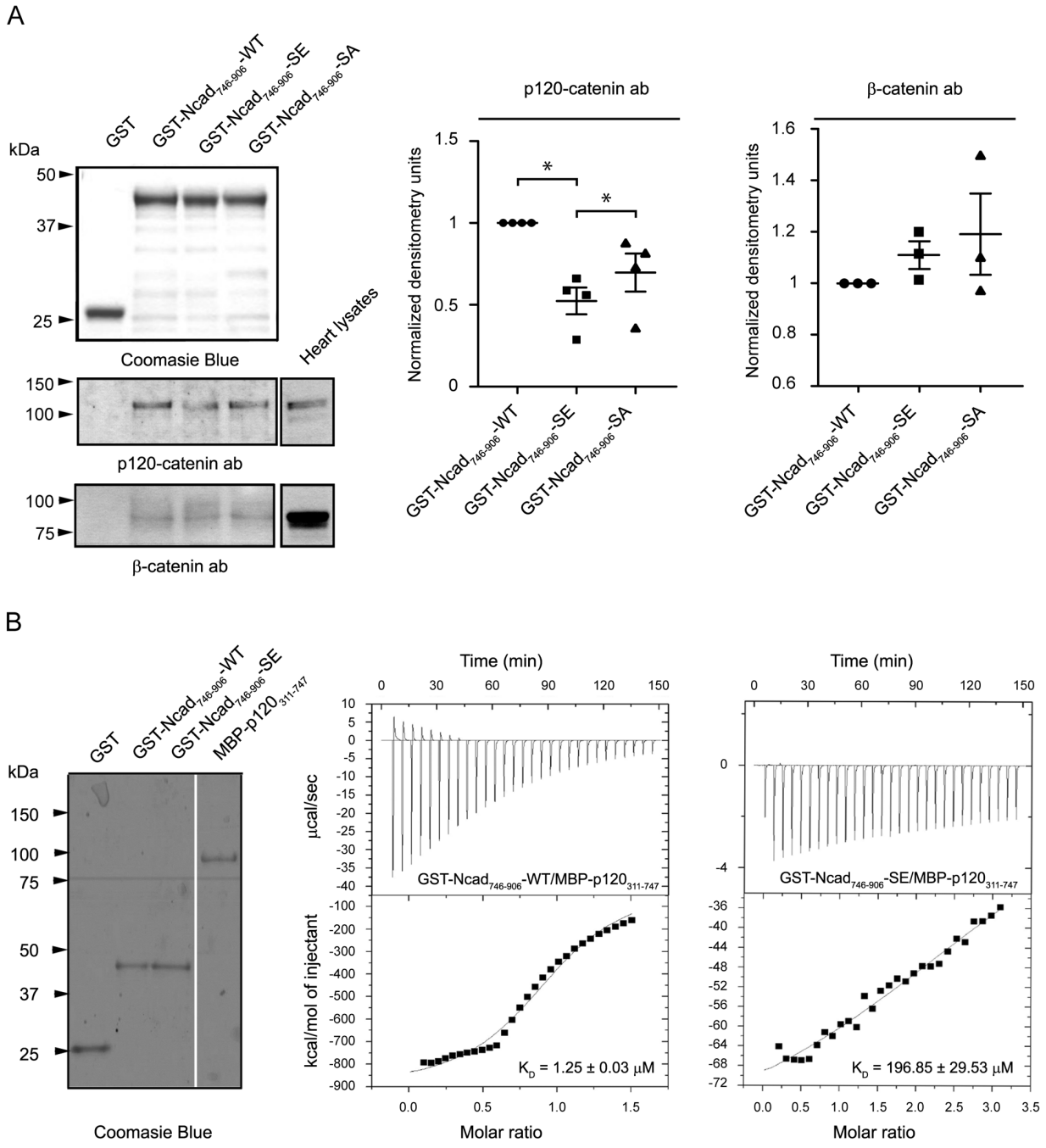

Figure 5: **Phosphorylation of N-cadherin at Ser-788 results in reduced binding to P120-catenin**. **A:** Equivalent amounts of recombinant GST-tagged wild type (GST-Ncad$_{746-906}$-WT), phosphomimic (GST-Ncad$_{746-906}$-SE), and phosphoablated (GST-Ncad$_{746-906}$-SA) N-cadherin proteins containing the cytoplasmic domain along with control GST-protein, as shown by Commassie Blue staining, were tested in pull down assays for their ability to precipitate and retain

endogenous p120-catenin from adult mouse cardiac lysates. Phosphomimic GST-Ncad$_{746-906}$-SE exhibited significantly reduced binding to p120-catenin compared to wild type GST-Ncad$_{746-906}$-WT and phosphoablated GST-Ncad$_{746-906}$-SA proteins; n=4, the binding of p120-catenin to GST-Ncad$_{746-906}$-WT was set to 1, while binding of p120-catenin to either GST-Ncad$_{746-906}$-SE or GST-Ncad$_{746-906}$-SA was normalized to GST-Ncad$_{746-906}$-WT. Statistical evaluation was performed with repeated measures one-way ANOVA followed by Tukey's multiple comparisons test; p=0.0203 for comparison of GST-Ncad$_{746-906}$-SE *vs* Ncad$_{746-906}$-WT and p=0.0496 for comparison of GST-Ncad$_{746-906}$-SE *vs* GST-Ncad$_{746-906}$-SA. This effect was specific to p120-catenin, as binding of β-catenin to GST-Ncad$_{746-906}$-WT, GST-Ncad$_{746-906}$-SE or GST-Ncad$_{746-906}$-SA was unaltered; n=3, statistical significance was determined with repeated measures one-way ANOVA followed by Tukey's multiple comparisons test. Non-continuous lanes are separated with white space (please see Supporting Information). **B:** Coomassie Blue staining showing recombinant GST, GST-Ncad$_{746-906}$-WT, GST-N-cad$_{746-906}$-SE and MBP-p120-catenin$_{311-747}$ that were used in isothermal calorimetry experiments; non-continuous lanes are separated with white space (please see Supporting Information). An average binding affinity, K_D, of 1.25 $\pm$ 0.03 μM was determined for GST-Ncad$_{746-906}$-WT and MBP-p120-catenin$_{311-747}$, whereas a K_D, of 196.85 $\pm$ 29.53 μM was calculated for GST-Ncad$_{746-906}$-SE and MBP-p120-catenin$_{311-747}$, consistent with the decreased binding observed in the pull-down assays; n=3 independent ITC experiments. Data are expressed as mean $\pm$ SEM; *: indicates statistical significance.

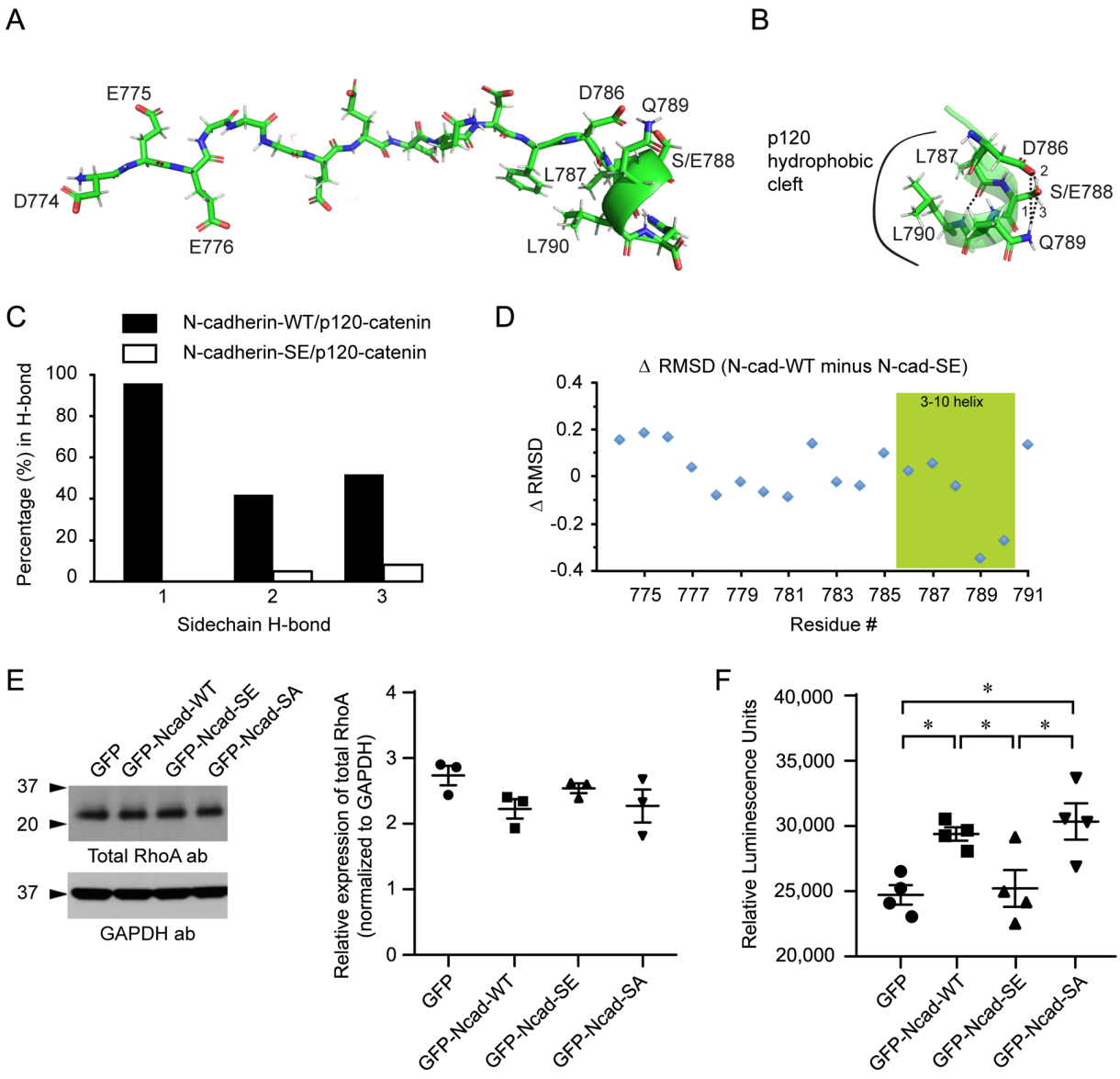

Figure 6: Impact of the N-cadherin/p120-catenin binding on RhoA activity. A: Model of the p120-catenin bound N-cadherin D774-H791 fragment, based on the p120-catenin/E-cadherin structure (PDB: 3L6X), showing an extended conformation with a COOH-terminal 3-10 helix. **B-C:** When the phosphomimic E778 is included into molecular dynamic simulations of this p120-catenin/N-cadherin complex, the 3-10 helix that supports hydrophobic interactions with p120-catenin loses multiple stabilizing hydrogen bonds. **D:** This loss of hydrogen bonds destabilizes the helix, resulting in more motion and weaker interactions with the corresponding hydrophobic patch

on p120-catenin, relative to simulations performed on the WT complex. **E:** Representative immunoblot using protein lysates prepared from HEK293 cells transfected with control GFP or full length wild type (GFP-Ncad-WT), phosphomimic (GFP-Ncad-SE) or phosphoablated (GFP-Ncad-SA) N-cadherin constructs indicate similar levels of total RhoA across all groups; GAPDH was used as loading control, n=3, data are expressed as mean $\pm$ SEM and one-way ANOVA followed by Fisher's LSD test was used for statistical evaluation. **F:** Measurement of GTP-RhoA levels (i.e., active RhoA) using luminescence-based G-LISA indicated that overexpression of phosphoablated GFP-Ncad-SA in HEK293 cells results in significantly increased RhoA activity compared to GFP and GFP-Ncad-SE; of note, GFP-Ncad-WT behaves similarly with GFP-Ncad-SA; n=4 experiments performed in duplicates. Data are expressed as mean $\pm$ SEM and statistical evaluation was done with one-way ANOVA followed by a Fisher's LSD test; p=0.0104 for GFP *vs* GFP-Ncad-WT, p=0.0189 for GFP-Ncad-WT *vs* GFP-Ncad-SE, p=0.006 for GFP-Ncad-SE *vs* GFP-Ncad-SA and p=0.0033 for GFP *vs* GFP-Ncad-SA; * indicates statistical significance.

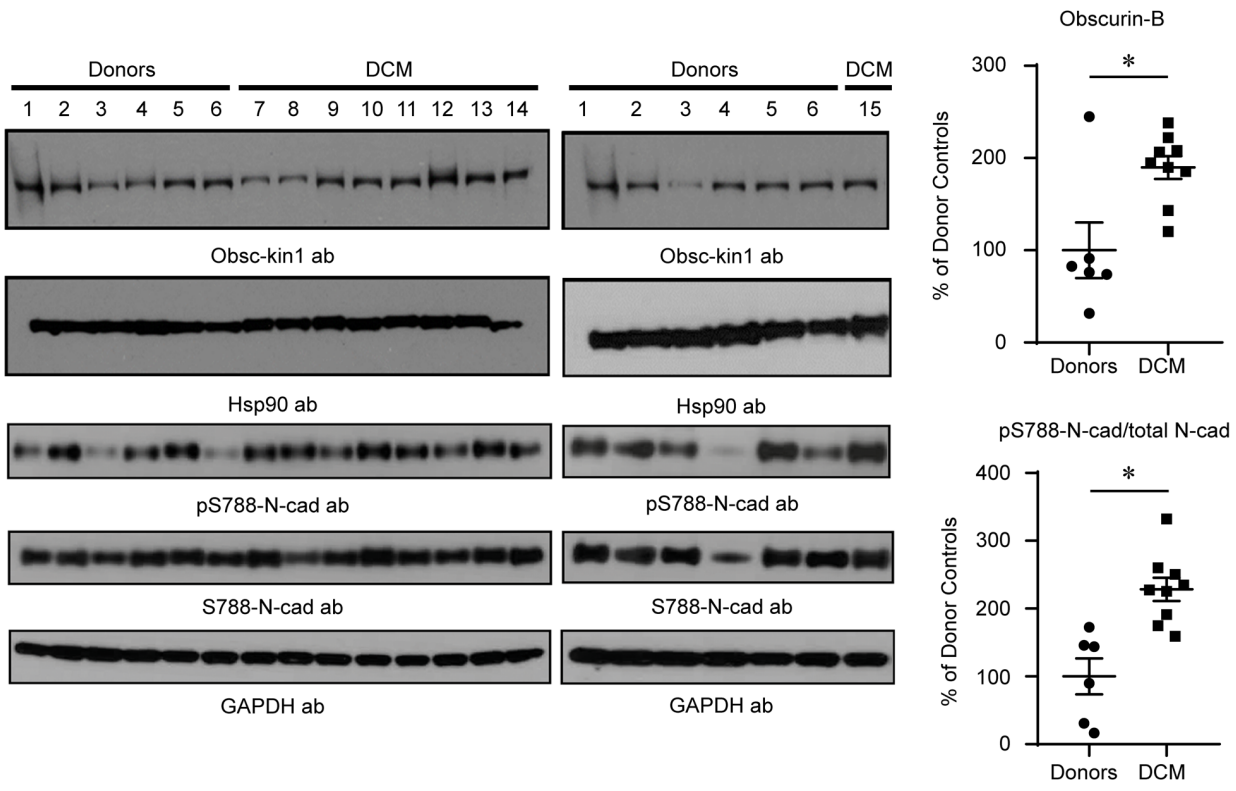

Figure 7: The obscurin-kin1/phospho-N-cadherin axis is upregulated in end-stage heart failure. Immunoblot analysis of protein lysates prepared from donor (lanes 1-6) and end-stage heart failure DCM (lanes 7-15) biopsies using antibodies to obscurin-kin1, phospho-N-cadherin-S788 and total N-cadherin-S788; GAPDH was used as loading control. Densitometric evaluation of the respective immunoreactive bands indicated that the levels of obscurin B containing kin1 and the ratio of phospho-N-cadherin-S788 to total N-cadherin are significantly upregulated in DCM samples compared to donor controls, following normalization to GAPDH which served as loading control; n=6 control donor biopsies and n=9 DCM biopsies run in triplicate; unpaired two-tailed t-test followed by Mann Whitney post-hoc test, data are expressed as mean $\pm$ SEM, p=0.036 for obscurin-B and p=0.0008 for phospho-N-cadherin-S788/total N-cadherin ratio; * indicates statistical significance.

Table 1: Characteristics of control donors and end-stage heart failure patients.

Patient Sample Code-University of Sydney Databank	Sample Numbering-Current Study	Diagnosis	Sex	Age	NYHA	LVEF	LVESD	LVEDD	FS	CAD	Clinical Presentation/ Cause of Death
Donor Control Samples											
4.083/4	1	-	M	53	-	-	-	-	-	-	Intracranial hemorrhage
7.054	2	-	M	33	-	-	-	-	-	-	Hypoxic brain injury
5.086	3	-	M	29	-	-	-	-	-	-	Hypoxic brain injury
5.128	4	-	M	45	-	-	-	-	-	-	Subarachnoid hemorrhage
6.048	5	-	F	54	-	-	-	-	-	-	Subarachnoid hemorrhage
7.044	6	-	M	63	-	-	-	-	-	-	Hypoxic brain injury
DCM End-Stage Heart Failure Samples											
2.066	7	DCM	M	43	IV	10	63	70	10	No	Interstitial fibrosis; No inflammation
4.058	8	DCM	M	64	IV	-	71	79	10	-	AF; Recurrent VT; LVAD; Chronic renal impairment
2.053	9	DCM	M	55	IV	6	-	-	-	No	AF; Aortic saddle embolism
3.085	10	DCM	F	53	III	20	59	74	-	No	Severely dilated LV; Mild RA dilation; Chronic AF; Mitral valve replacement
4.032	11	DCM	M	31	IV	10	92	100	-	-	Severely dilated LV; Mildly dilated LA; Hypokinetic RV
5.057	12	DCM	F	52	IV	10	86	95	8	No	AF; Decompensated biventricular failure; AICD/LVAD
5.060	13	DCM	M	54	III	34	56	77	35	No	Chronic AF; VT; AICD
5.062	14	DCM	F	62	IV	25	49	59	16	No	Chronic AF; AICD/LVAD
7.090	15	DCM	M	49	IV	10	58	60	9	No	Mild LV dilation with severe systolic dysfunction; AF with bi-atrial dilation; Pacemaker inserted

Abbreviations: DCM: Dilated Cardiomyopathy; F: female; M: Male; NYHA: New York Heart Association Classification; LVEF: Left Ventricular Ejection Fraction; LVESD: Left Ventricular End Systolic Diameter; LVEDD: Left Ventricular End Diastolic Diameter; FS: Fractional Shortening; CAD: Coronary Artery Disease; AF: Atrial Fibrillation; VT: Ventricular Tachycardia; LV: Left Ventricle; RV: Right Ventricle; LA: Left Atrium; RA: Right Atrium; LVAD: Left Ventricular Assist Device; AICD: Automatic Implantable Cardioverter-Defibrillator;-: not known.